university of groningen / faculty of science and engineering

Impact of Varied Cable Lengths on the Kinematics of a Point-Absorber Wave Energy Converter Model: An Experimental Investigation

BSc. Industrial Engineering and Management

Bachelor Integration Project

Author:
Demeter Koša: S4567269

Supervisors:
1st: Prof. Antonis Vakis
2nd: Mehran Mohebbi
Daily: Andreas Asiikkis

19th of January 2024

ABSTRACT

Ocean waves are an enticingly energy-dense renewable energy resource, yet Wave Energy Capture (WEC) systems remain an immature and underutilised technology. Point-absorber WECs are amongst the most highly-developed type of WEC, popular for their relative simplicity, amongst other reasons. They are typically designed to capture energy in the Heave direction, but face complex resonance-control challenges to make them effective. Surge-based PA-WECs are under-explored in literature, and their potential for simple control - and therefore effective energy capture in practice - is unknown.
In their numerical study, [Asiikkis et al., 2023] produced results which suggest that cable length may be an effective tuning parameter for the maximisation of surge amplitude. The research in this paper attempts to experimentally validate the theoretical results. Furthermore, as it is exploratory in nature, the research aims to uncover and explain any other trends of behaviour that are observed.
The research is conducted by constructing a model moored floater and subjecting it to various cable length and wave conditions in a wave flume, and measuring its response. In total, 9 cable lengths were tested across 6 wave conditions of increasing frequency and height, and 3 trials were conducted for each set of conditions. The floater's kinematic responses were recorded with a video camera, and wave conditions were measured via an ultrasonic sensor. The gathered data was then processed using custom MATLAB scripts, and Minitab was employed for subsequent data analysis.

Significant evidence supporting some of the findings laid out by [Asiikkis et al., 2023] was found. In particular, an indirect causal connection was found between cable length and surge amplitude: a change in cable length caused a change in the harmonic frequency of the floater with respect to the incident waves, and a harmonic frequency of half the wave frequency consistently maximised surge amplitude. Therefore, cable length was shown to be an effective tuning parameter for the optimisation of surge behaviour, for the case where maximal surge amplitude is desirable.
However, contrary to the theoretical results, no inverse relationship between surge and heave amplitudes was observed. Despite this, a comprehensive explanation for the observed trend in heave amplitude was developed.
Moreover, a strong linear relationship was discovered between surge amplitude and the variable 'surge velocity per wave frequency', when grouped by harmonic response. The potential applications of this relationship were explored.

Overall, the behavioural trends detailed in this study serve two purposes: to reinforce the prospect of using cable length as a tuning parameter for future surge-based PA-WECs, and to invite further research to explore the persistently ill-understood concepts.

CONTENTS

1 INTRODUCTION

The problem of climate change calls for a global shift from fossil fuels towards renewable energy sources. Ocean waves are amongst the most energy-dense sources of renewable energy, and are arguably underutilised due to the challenging ocean environment. The research field of Wave Energy Converters (WECs) offers a multitude of promising instruments for renewable wave-energy harvesting. One such instrument, called a point absorber, involves a floating element connected to the sea floor with a cable, which generates energy via the movement of the floater. Typically the focus is on the vertical (Heave) movement of the floater. However, energy could theoretically also be generated through the horizontal (Surge) movement.

One study by [Asiikkis et al., 2023] investigates the potential of surge-based point-absorbers for energy generation by attempting to maximise the surge amplitude through adaptable cable tightening. The study outlines the floaters' behavioural trends with increasing cable tension, and successfully identifies a series of optimal cable tensions for various sea states. This research, however, as with most research into WECs, is strictly theoretical and simulation-based. Whilst modern WEC models, such as the popular and open-source WEC-sim [Ogden et al., 2022], are ever-increasing in accuracy, speed and external validity, the value of small-scale experimental testing can be recognised in their validation of simulation results and for stand-alone simple testing.

In this paper an experimental approach is taken to investigate the effect changing cable length has on the surge behaviour of a moored floater. Being that the focus of WEC research is primarily simulation-based, and in the case of point absorbers it is focused on the Heave motion, this study will shed light on the understudied Surge behaviour of point absorbers with varying cable length, and will contribute useful insights into floater behaviour, including data on ideal cable length for maximal surge amplitude.

In Chapter 2, the paper investigates and explains the context of the problem, and develops a detailed description of the experimental system. The specific objectives of the research are defined, and the research questions are developed. Then in Chapter 3, pilot testing is performed and the lessons learned from it are subsequently used to improve the experimental setup, which is described extensively in Chapter 4. Chapter 5 details the methodology, from experimental procedure, to data processing using MATLAB, and to data analysis and cleaning using Microsoft Excel and Minitab. Chapter 6 contains the results and discussions, which are followed by a brief mention of the limitations of the research in Chapter 7, and the subsequent recommended directions for future research in Chapter 8. Finally, Chapter 9 concludes the research paper.

Figure 1.1: An operational point-absorber wave-energy-converter deployed by Enel Green Power in Chile, 2021 [WEC, 2021].

2 PROBLEM CONTEXT

2.1 Technical Context

Point-absorber-type WECs (PA-WECs) typically consist of a floater, a mooring system, and a power take-off system (PTO). The floater resides on the ocean surface, and is secured in place relative to the ocean floor via the mooring system. The device captures energy from incoming waves by translating the kinetic energy imparted onto the floater into electrical energy, via the PTO.

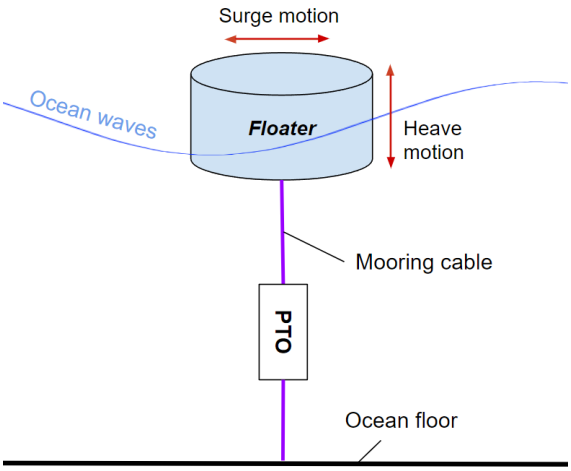

Figure 2.1: An elementary schematic of a Point-Absorber Wave Energy Converter

A WEC tends to most effectively capture energy from waves when its fundamental frequency matches the incident wave frequencies - i.e. it achieves resonance [Li and Yu, 2012]. Therefore, the energy efficiency of a WEC depends largely on how well its fundamental frequency matches the environment. This fundamental frequency is inextricably linked to its physical properties which can be varied in any number of parameters: shape, size, weight, draft, material, the cable(s) can consist of any of an infinite spectrum of possible cable arrangements, lengths, tightnesses or elasticities. The PTO system introduces a further myriad of complexity into the already highly-interconnected system.

The tweaking of these parameters is a complex problem of system optimisation, and is one of the primary areas of study for WECs. These promising renewable-energy-capture devices have proved to be deceptively challenging, and the technology remains immature compared to other renewable energy sources [Mwasilu and Jung, 2019]. Due to this immaturity, there is no clear agreement yet on optimal energy extraction strategies ([Drew et al., 2009]). To date, research has primarily been focused on exploiting the 'Heave' motion of floaters, with little attention being given to the Surge motion.

The lack of literature on Surge-based PA-WECs highlights a research gap in the field. Surge-based systems may have currently-unknown advantages over typical Heave-based systems, which may then have implications for future PA-WEC designs. This paper aims to explore this research gap.

2.2 Ocean Grazer Project & Related Research

Ocean Grazer B.V. is a company collaborating with researchers in the CMME[1] research group at ENTEG[2] in the RUG[3], working to develop WEC technology as a component of its larger offshore renewable energy harvesting and storing farm, dubbed the Ocean Grazer (OG). The OG project is still in early development, with concept WEC designs and power take-off (PTO) systems being investigated ([Wei et al., 2017],[Bechlenberg et al., 2023]).

While investigating the effects varying parameters have on the behaviour of a PA-WEC, PhD candidate Andreas Asiikkis (working with the CMME group) identified mooring-cable tightness as a potentially influential parameter. The resulting paper, [Asiikkis et al., 2023], investigates the effects of tightening the mooring cables on the Surge response of a floater, primarily using WEC-sim (a popular WEC simulator [Ogden et al., 2022]) to obtain theoretical results, and also performing some limited physical experiments to obtain initial validation for the models.

The research paper obtains results that "suggest that an optimum value exists for the unstretched [cable] length where the amplitude of Surge motion can be maximized, providing a potential tuning parameter for enhancing wave energy capture in the Surge direction". Furthermore, a positive relationship was reported between the period of incident waves and the optimal unstretched cable length. The paper then demonstrated that experimental validation of these results was both possible and valuable.

This paper aims to build upon this previous research by improving the experimental design, and carrying out rigorous testing with extensive data analysis to obtain meaningful and useful empirical data, which will be compared against the theoretical results.

2.3 System description

Due to the complexity of moored-floater systems, a visual depiction of the system - and the general procedure used in this paper to study it - has been drawn in Figure 2.2.

The elements to the left and bottom of the system boundary are a (non-exhaustive) list of parameters which are thought to affect the behavioural properties of a moored floater ([Guo et al., 2022]). They are under the category of external factors, and include the *internal* and *external conditions*. The internal conditions consist of geometric parameters, the setup parameters, and the material choices, each of which are composed of (but are not necessarily limited to) the items branching from them. The same is true for the wave parameters in the external conditions category. Causal relationships between parameters are indicated by

[1]Computational Mechanics and Materials Engineering
[2]Engineering and Technology institute Groningen
[3]Rijksuniversiteit Groningen (University of Groningen)

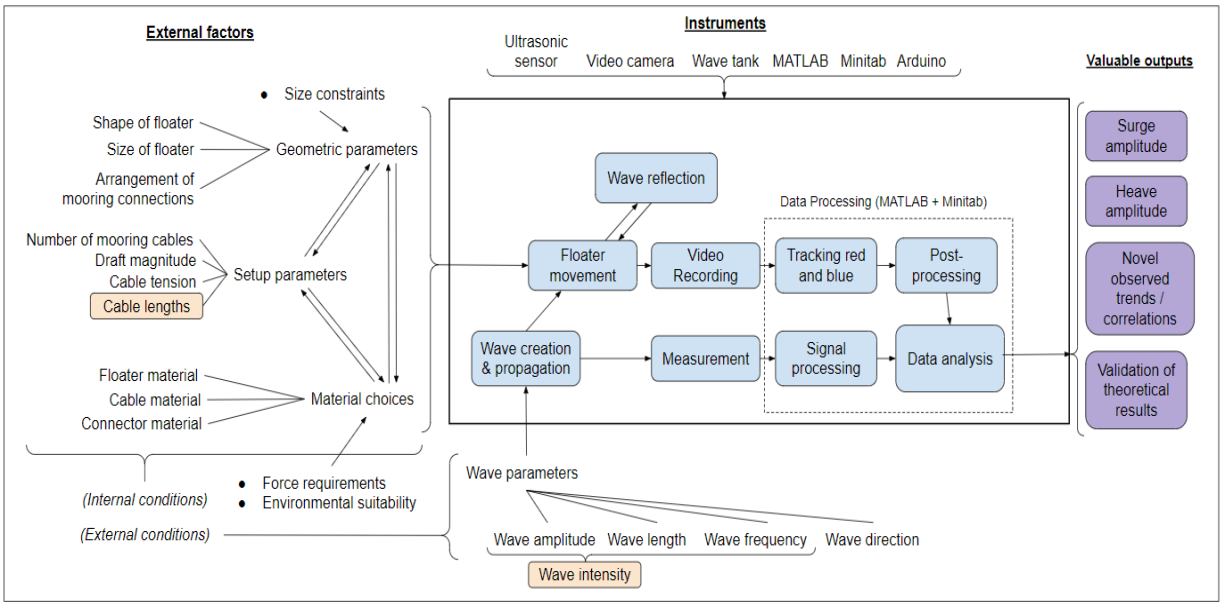

Figure 2.2: Diagram of the system, including external inputs, performance metrics and instruments used. Lines represent component parts, arrows represent causal relationships, and the box represents the system boundary.

directed arrows[4]. Size constraints (due to the wave flume width), force requirements, and environmental suitability (saltwater environment) influence the geometric parameters and material choices. The main instruments used for the experiment are: ultrasonic sensors, a video camera, a wave flume, MATLAB for signal processing, Minitab for data analysis, and Arduino.

Within the system boundary, the wave parameters determine the type of wave created. In response to both the wave conditions and the given parameters, the floater moves. Wave reflection from the end of the wave flume, as well waves reflecting off the floater itself and bouncing back off the wave flume walls, causes some feedback interference. The motion response of the floater is recorded using a video camera, and the wave profile is recorded using two ultrasonic sensors. These signals are processed using MATLAB, and the refined data is analysed in Minitab. Although more sophisticated testing methods exist (for example: [Bacelli et al., 2019], [Holmes, 2009]), this is the technology available for the project, and is sufficient.

The primary purpose of this study is to validate the theoretical research in [Asiikkis et al., 2023], and to gain as comprehensive an understanding of moored-floater Surge behaviour as possible. Therefore, the independent variables (indicated in orange) are the **Cable length**[5] and **Wave Intensity**. The valuable outputs of this study

[4]This is not a complete description; some causal relationships, such as between cable length and cable tension, are omitted to reduce complexity, and some relationships are entirely unknown.

[5]Variables will be written in **bold** throughout the paper once they are identified, to improve readability.

are Surge and Heave **Amplitude** data with respect to changing **Cable length** under various wave conditions, as well as any novel trends/correlations that are observed from the data.

2.4 Research objective

The research objective is to: obtain knowledge on point absorber behaviour, and validate theoretical research, by creating a proficient physical model and using it to experimentally investigate the effect of changing **Cable length** on the resulting floater kinematics (with a particular focus on maximising Surge **Amplitude**), within 3 months.

2.5 Research questions

The main research question is: What are the behavioural trends of a moored floater, with a particular focus on maximising Surge **Amplitude**, under varying **Cable length** and wave conditions?

The main research question can be broken down into the following component subquestions:

1. **SQ1**: What requirements constitute a "proficient" physical PA-WEC model, as well as the measurement system used to track it, and what limitations exist for their creation?

2. **SQ2**: What observations can be made about the Surge behaviour of the model PA-WEC from the gathered data?
    - **SQ2.1**: What observations can be made about the behaviour of the model floater in other degrees of freedom?

3. **SQ3**: To what extent do the empirical results support or oppose the findings of the theoretical research in [Asiikkis et al., 2023]?

3 PILOT TESTING

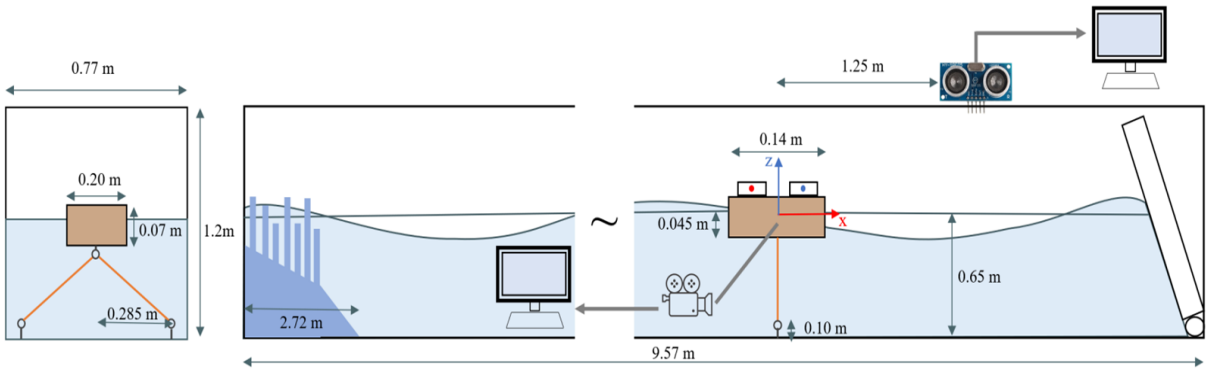

Figure 3.1: Depiction of the experimental setup used in the pilot stage. The wave flume is shown along the wave-travel axis on the left, and parallel to wave-travel axis on the right. (Image courtesy of [Asiikkis et al., 2023]).

First, pilot testing is conducted in order to gather information on the proficiency of the existing experimental setup, identify flaws, and implement improvements.

Pilot testing involved using the same physical model, sensing methods, and data processing used by [Asiikkis et al., 2023] (see Figure 3.1 for the experimental schematic). In total, 1 cable length was tested across 13 wave conditions of increasing intensity. It was demonstrated that the experimental setup is capable of tracking the floater, but there are severe limitations which need to be addressed. Namely:

- The short floater height (70mm) limits the draft capacity, and subsequently the range of testable wave heights.
- The floater demonstrates considerable yaw and roll behaviour. This is undesirable as it is a) difficult to measure, and b) introduces unknown hydrodynamic complexities, which are outside the scope of this project.
- The mooring cables are inaccessible, which makes length measurement impossible and adjustment laborious.
- The existing waterproof tape coating is ineffective. Water inside the floater influences the mass - and subsequently the behaviour - of the floater, to an unknown degree.
- The colour-tracking script experienced high levels of colour interference, where unwanted blue or red pixels were identified. Extensive manual adjustment was

required during processing to account for this. Furthermore, the processing speed was extremely slow. These issues proved to be considerably problematic, and must be minimised for full-scale testing.

4 MATERIALS

The following section expounds upon the technical specifications of the materials used for experimentation. Firstly, the wave flume and its various components are described. Secondly, the learning points obtained during pilot testing (see section 3) are used to generate design requirements, from which design choices are made and the new floater is built. Then, the cable system is similarly improved upon. Lastly, the video and ultrasonic sensors, and their positions in the experiment, are detailed. Extensive measures are taken to improve the lighting and colour conditions for the camera sensing element, to avoid colour interference.

4.1 The Wave Flume

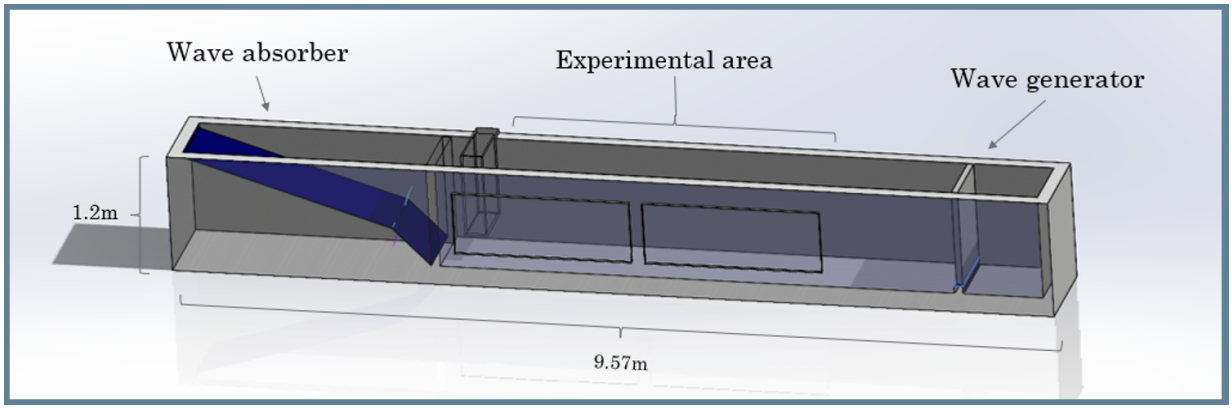

Figure 4.1: A minimal model of the wave flume used for this research, provided by the Engineering and Technology Institute Groningen. Note: see Appendix Figure 1 for detailed dimensions of the wave flume.

The wave flume used for this research is composed of a wave generator, an experimentation area, and a wave-absorbing beach.

The wave generator
The wave generator consists of a motor, which powers a crankshaft connected to the top of a large paddle. The large paddle fits snugly into the right-most end of the wave flume, and has a pivot connection at its base. When the motor spins, the rotational motion is

translated into angular oscillations of the paddle, which generate water waves. A single adjustable dial with a corresponding digital readout controls the speed (rpm) of the motor, which in turn controls the oscillation frequency (Hz) of the paddle. The digital readout gives values to one decimal place, which are dimensionless but correlate linearly with the output frequency of the paddle.

Since an increase in paddle oscillation frequency creates waves with increasing intensity (i.e. higher **Wave Frequency** (W_f) [Hz] and **Wave Height** (W_h) [m], but to an unknown degree), the value of the digital readout is used as a measure of the "**Wave Intensity** (W_i) [$dmnl$]".

The experimentation area
The experimentation area features two viewing windows, and is equipped with carabiners fixed to a sandy base. The position of the carabiners is adjustable along the long axis of the wave flume, as they are attached to a rail. They are $0.68m$ apart, centred relative to the walls of the tank, and provide ideal connection points for mooring cables.

The wave-absorbing beach
The wave-absorbing beach acts to absorb the energy of the waves, so that waves are not reflected back towards the experimentation area. However, [van Luijk, 2023] found that the beach is imperfect, and at wave frequencies of $\geq 1.15Hz$ there are significant wave reflections. Therefore, while this does limit the range of experimentable frequencies for the project, these higher wave frequencies will be avoided for the sake of validity.

4.2 Building the New Floater

Following from the learning points of the pilot testing, the model floater has these requirements:

1. Width: Fit within walls of the wave flume (0.77m), with adequate space to spare (to minimise reflection interference from walls).
2. Height: Tall enough to allow for a greater range of draft and wave conditions, but not so great that it compromises stability.
3. Stability: Include two cable connection points perpendicular to the wave motion, rather than a single central connection, to discourage yaw and roll behaviour.
4. Waterproofing: The floater needs to be adequately waterproof for at least the duration of the experiments (3 weeks).

To address these requirements, the new floater was designed as a 204x204x204mm hollow acrylic box. These dimensions meet the specifications, leaving a gap of 283mm between the

floater and the wave flume walls, and allowing for an experimentally valid draft of up to 150mm ($> 3\times$ improvement on the previous 40mm limit).
The 3mm thick acrylic was laser-cut with two finger joints on each side, and glued together using acrylic binder which ensures structural integrity. For extra waterproofing, the seams were sealed on the inside with hot glue.
Two connectors were secured using super glue. They are positioned along the pitch axis, equidistant from the edges at 34mm.
Additionally, the acrylic box design allows for the customisation of other internal conditions, such as mass adjustment, density, mass distribution, or even potentially PTO integration, which opens the door for future studies to be made with it. In this case, the box was filled with wood to maintain a similar density to the previous wooden floater. However, it was too top-heavy and therefore unstable, so the two uppermost planks were removed during testing to lower the centre of gravity. The two floaters can be seen side by side in Figure 4.2.

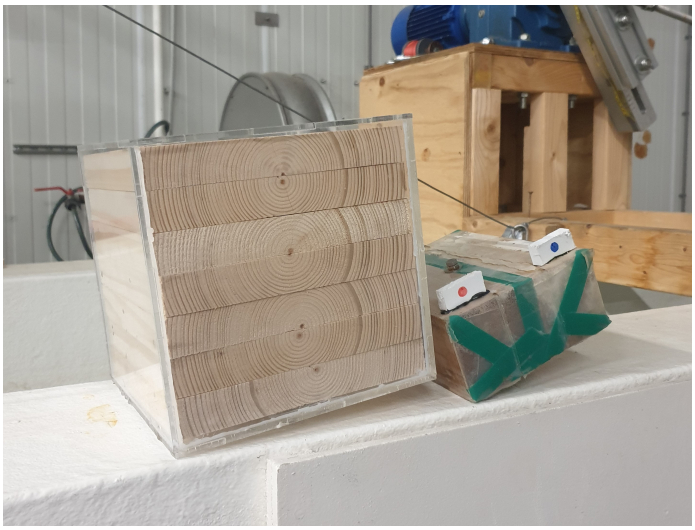

Figure 4.2: The new floater (left) side by side with the old floater (right).

4.3 The Cable System

To conduct experiments where the mooring cable length is an independent variable, the cables need to be easily, reliably, consistently, and measurably adjustable in length.

Consistency

Since there are two connection points, the two cables need to ideally be identical in length, which is problematic when making adjustments. It is virtually impossible to ensure that both cables are always equal.
To solve this problem, the two cables can be combined into a single cable spanning both connection points. This way a single length adjustment can be made to change both cable

Figure 4.3: The cable configuration, with a bowline knot on the left (for its strength), connected through both connectors to the tarbuck knot on the right, with the regular interval markings visible. (Note that the right connector is substituted with tape in this image, but normally it is identical to the left connector).

lengths. The floater then needs only to be centred in the middle of the cables, which halves the potential for measurement error and simplifies the process.

Accessibility and Reliability

During testing, the cables are submerged and difficult to access. Performing adjustments by first removing the floater and cables would make reliable adjustments easier, but it would also require either draining and refilling the wave flume, or having to fully enter the water each time. To avoid this, a system needed to be devised where adjustments could be easily possible from outside of the wave flume.

The solution is found in a tarbuck knot, which is a 'slide and grip loop' knot, meaning that it creates a loop whose size is adjustable by hand, but will lock firmly in place under a sudden load. Applying this knot to one side of the mooring configuration provides exactly the characteristics needed: easy to adjust and reliably secure.

Adjustable cable length
Due to the slight elasticity of the cables, their curvature in knots, and their inaccessibility during testing, the exact lengths of the cables are difficult to measure. Attempting to measure their lengths would only serve to invite errors and compromise validity.
Fortunately, the exact lengths are less relevant than the *changes* in length[1]. Therefore, the cable was marked at regular intervals along the line with the tarbuck knot, so that the knot could be moved to each line, producing repeatable changes in length. The intervals are 36mm apart, which corresponds to a 9mm change in cable length per cable. This was chosen because it gives approximately a 10mm change in draft, and allows for a draft range of 40mm, 50mm, 60mm, ... , 190mm, 200mm to be tested.

Cable characteristics
Offshore WECs typically use mooring configurations which possess a degree of elasticity, to reduce peak loads and increase longevity ([Xu et al., 2019],[Weller et al., 2015]). However, elastic mooring cables are undesirable for this experiment as they would introduce unknown dynamic effects, which are outside of the scope of this study. Therefore, a highly-stiff braided polypropylene rope of 4mm diameter was chosen. In addition to stiffness, it possesses the required degree of marine durability, and knotability. The cable is white in colour, so as to not interfere with colour-tracking sensors (Section 4.4), and for ease of marking with permanent markers.

4.4 The Sensors
The experiment requires two types of sensors: 1) a camera, to record the motion of the floater, and 2) at least one ultrasonic sensor, to detect the surface elevation of the water. The full experimental setup can be seen in Figure 4.4.

[1]Knowing the exact configuration of cable lengths and wave profile to give the largest surge magnitude is useful only for this floater; any floater with slightly different characteristics will probably have a different optimal configuration. What is really valuable is finding out what the trends in behaviour are, and whether there is such a thing as an optimal configuration at all.

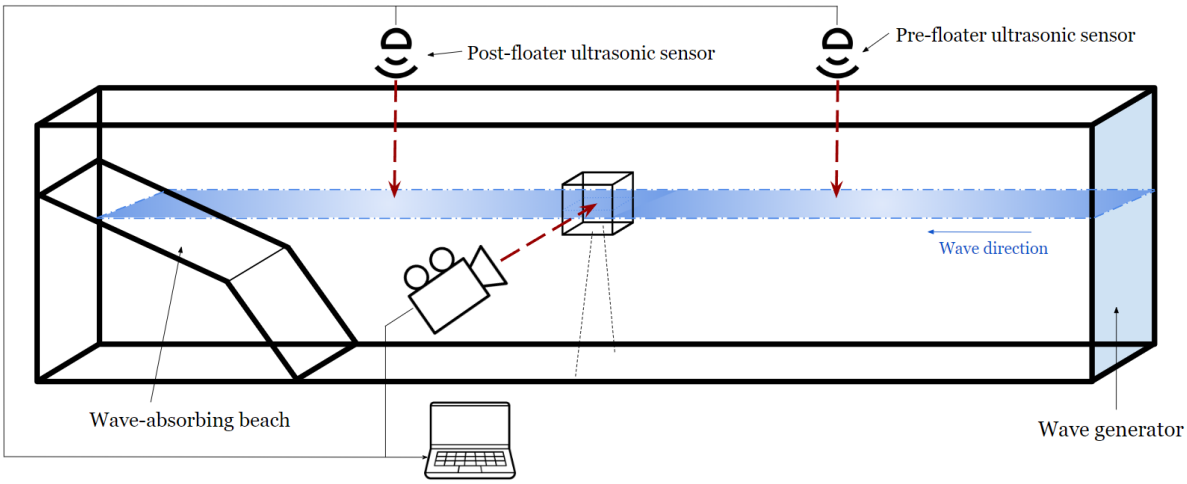

Figure 4.4: A graphical representation of the complete experimental setup. The largest cuboid represents the wave flume. The wave generator is located on the rightmost wall of the wave flume, and the wave direction is to the left. Two ultrasonic sensors are visible above, pointing down at the surface. The floater (small cube) is moored by two lines, with the axis of the mooring points on both the floater and flume base being perpendicular to wave direction. The camera is aimed directly at the floater. All sensors are plugged into a laptop. The wave absorbing beach can be seen on the left. The image is not to scale.

Video camera

The video camera operated at a frame-rate of 16.5 frames per second, and a resolution of 1080x1920 pixels. It was positioned to look through the viewing window on the side of the wave flume, approximately in line with the geometric centre of the floater when at steady-state, and at a draft of 80mm. The camera was kept fixed in this position for all experiments.

To detect the floater movement over time, the floater was given one red and one blue marker. Afterwards, image processing is used to detect the red and blue pixels in each frame, and thereby track the floater movement. Previously there was much colour interference, where unwanted red and blue pixels were identified aside from the floater, destroying the data or requiring intensive video editing to remove.
To resolve this, several actions were taken:

- Ideal lighting conditions were tested for, and implemented.
- Larger and more vibrantly coloured dots were applied on the floater.
- The camera was moved closer to the floater.
- Reflections from the glass window of the wave flume were minimised by hanging up an opaque matte curtain behind the camera.
- Any coloured surfaces within the frame were covered with white paper or green tape.

The result can be seen in Figure 4.6, which can be compared to the messier view seen in Figure 4.5.

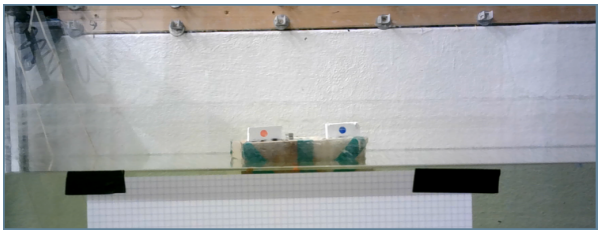

Figure 4.5: The point of view of the camera in the pilot testing.

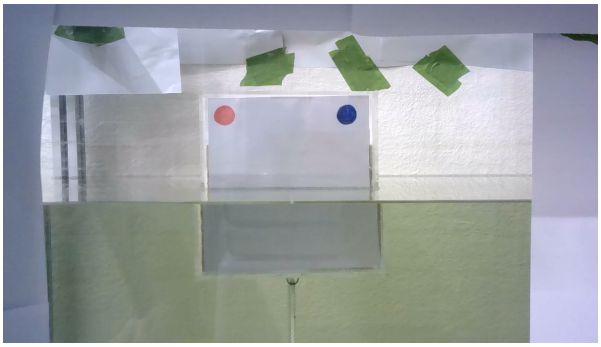

Figure 4.6: The improved view of the camera, with changes evident. The matte curtain lies behind the camera, out of view.

Ultrasonic sensors

Ultrasonic sensors were applied both to the right and left of the floater, to measure the surface elevation of waves before (labelled 'pre-floater') and after ('post-floater') the waves make contact with the floater, respectively. In flat-water conditions, they were 0.24m above the surface of the water. They measure the wave height every 10ms (therefore operating at 100Hz), and to a resolution of 0.01m. The post-floater ultrasonic sensor is pictured in Figure 4.7. Note that, for this experiment, only the data from the pre-floater ultrasonic sensor is utilised. The post-floater ultrasonic sensor was installed only to gather additional data to be archived for potential future studies on other phenomena. However, for this project, the use of that data is deemed outside of the scope.

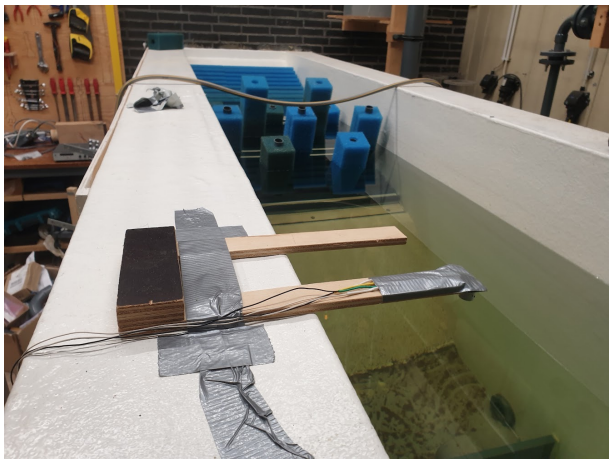

Figure 4.7: A view of the post-floater ultrasonic sensor, secured over the water and pointing vertically down. The wave-absorbing beach can be seen in the background, and the floater is located behind the camera.

5 METHODOLOGY

5.1 Experimentation procedure

The floater was set up in the wave flume at an initial **Cable length** of 0.659m, which gives a **Draft** of 80mm. This was chosen because 80mm is the natural **Draft** of the floater at steady-state under its own mass and buoyancy, therefore this **Cable length** is the most neutral position and any subsequent changes made to the **Cable length** are made relative to the neutral position. Due to polypropylene's tendency to stretch slightly in water, the cables were given 24 hours to settle, and then were readjusted.

This is the full experimental procedure: Once the ultrasonic sensors and camera are fixed securely in their places to ensure reliable measurements, and connected to a laptop, testing begins. The wave generator is turned on and set to the desired **Wave Intensity**, and 2 minutes are given for the waves and the floater to reach steady state behaviour. Then, data is collected for (at least) 1 minute from all sensors at the same time. Once data collection ends, the wave generator is turned off, and several minutes are given for the movement to cease totally, while data files are named, labelled and saved. Once no movement is visible from either the water surface or the floater, the process is repeated for the next test.

For each of the 9 **Cable lengths**, 6 **Wave Intensities** were tested. For each combination of **Cable length** and **Wave Intensity**, three independent trials were performed for experimental validity. This totals to 162 individual trials.

5.2 Data processing

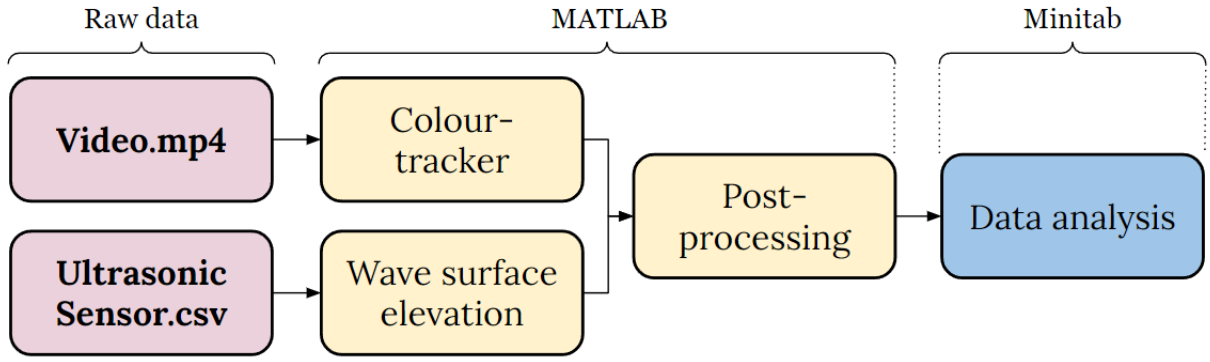

Figure 5.1: The steps followed during data processing, with flow of data indicated by arrows. Each red box represents a different raw data file type. Each yellow box represents a separate MATLAB script. The blue box represents the action of data analysis, performed using Minitab.

Data processing is carried out in a series of logical steps, detailed in Figure 5.1.

Firstly, the motion of the floater is extracted from the raw video files using an image-processing colour-tracking script written in MATLAB. Secondly, also using a MATLAB script, the wave-surface-elevation measurements are processed to calculate the wave frequency, period, and wave height. Then, the obtained data is fed into a post-processing MATLAB script, which performs further calculations, creates relevant plots, and collates the data into tables. These tables are then exported to Microsoft Excel and Minitab, where the data is validated and cleaned in the data analysis section. The following sections expand on the details of each step.

5.2.1 Colour-tracking

This project uses a customised version of the colour-tracking script developed by [Verma and Verma, 2019].
It works by identifying all pixels of a designated colour (above a specified intensity threshold) within a single frame, and calculating the mean location of those pixels. The location is saved as a Cartesian coordinate in an array. This task is performed for every frame in the video, finally outputting an array of coordinates which detail the 'path' of the coloured pixels. It performs one loop for red pixels, and another loop for blue. Then, the path of the midpoint position between the red and blue pixels is found:

```
pixelsMidpoint = (redPixels + bluePixels) / 2
```
(5.1)

In practice, the red and blue markers on the floater are located equidistant from the vertical axis. Therefore, the `pixelsMidpoint` array contains the path of the location of the vertical axis on the front face of the floater. The paths are displayed in Figure 5.2.
After analysing one video file, the collected data is saved, and the next video file is loaded.

5.2.2 Wave-surface-elevation

The ultrasonic sensor wave-surface-elevation measurements are processed using a fast-fourier transform, which decomposes the elevation signal into a spectrum of frequencies with varying amplitudes. From this, the dominant frequency is identified and the **Wave Frequency** $[W_f]$ (Hz) and **Wave Height** $[W_h]$ (m) data is recorded. Furthermore, the **Wave Period** $[P]$ (s) is calculated:

$$P = 1/W_f \tag{5.2}$$

The script loops over all ultrasonic sensor readings (in .csv files), and collates the extracted data in a single table.

5.2.3 Post-processing

The post-processing script utilises the colour-tracking and wave-surface-elevation script outputs to calculate key performance data.

As can be seen in Figure 5.2, the patterns of movement between points on the front face of the floater differ. Therefore, the point on the face that is chosen for tracking - the 'tracking

point' - influences various measurements. In reality, the tracking point may depend on the design and configuration of the PTO. Due to the lack of literature on surge-based PA-WEC designs, an informed decision cannot be made. Thus, for the purposes of this study, the tracking point is chosen to be the centre of mass (M_c) of the floater.

The advantage of this tracking point is that subsequent Surge and Heave measurements do not contain components of Pitch around the centre of mass, which would muddy the results. Furthermore, this choice, paired with the modular wooden mass design, allows for future research into how changes in the centre of mass affect the floater behaviour.

M_c is found by calculating the geometric centres of the box the wooden mass within the box, and finding the balance point between the two masses. This calculation assumes uniform density of the acrylic box and wooden mass, and perfect concentricity between them along the z-axis. The masses of glue, paper and cable connectors was considered negligible.

The projection of M_c on the front face of the floater is located 0.098m below the mid-point between the coloured markers. In the post-processing script, the coordinate location array of the known `pixelsMidpoint` is translated for both its x- and y-coordinates 0.098m downwards, and adjusting for the pitch angle θ:

$$\texttt{centreOfMassX = pixelsMidpointX + 0.098 *} \ \sin(\theta) \tag{5.3}$$

$$\texttt{centreOfMassY = pixelsMidpointY + 0.098 *} \ \cos(\theta) \tag{5.4}$$

The path data of M_c then analysed.
First, the **Amplitude** (A) [m] of the response in the Surge, Heave, Pitch and Yaw/Sway directions is calculated by finding the mean magnitude of the maximum and minimum peaks of the x- and y-components, and taking the difference:

$$\texttt{Amplitude = (mean(peaks max) - mean(peaks min))/2} \tag{5.5}$$

An example of identified maximum and minimum peaks can be seen in Figure 5.3.
Note that for the case of Yaw/Sway, the measurements are limited to a rough indication: The degree of Yaw/Sway is measured by calculating the difference between the known standard distance of the coloured markers (0.1400m) and the observed distance; if the observed distance is smaller, the floater will have either rotated in the Yaw direction, or moved away from the camera, exhibiting Sway. The degree of Yaw does not change linearly with the angle of rotation, the direction of Yaw is unknown, and the component of Sway is unknown. Therefore, 'Marker distance change' [Δd] (m) is an indicator variable, and not a direct measurement of Yaw or Sway.

Second, the time-spans between individual peaks are calculated, and are used for two purposes:

1. to approximate the period of the response (by finding the mean time-spans, which are saved as **Max peaks period mean** ($M_{\overline{x}}$) [s] and **Min peaks period mean** ($N_{\overline{x}}$) [s]), and

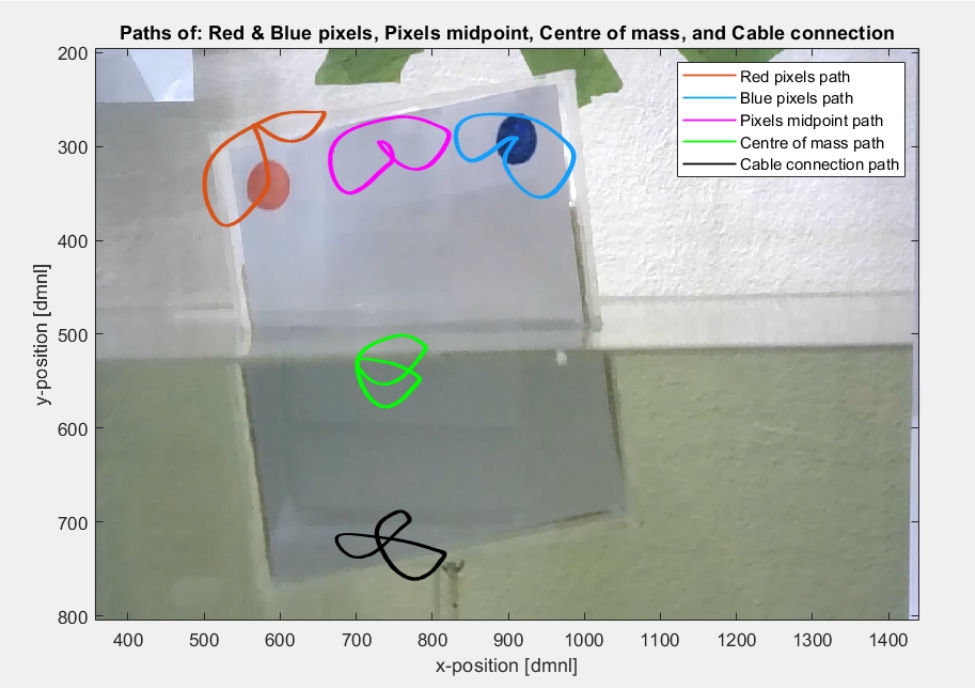

Figure 5.2: A still-frame image of the floater during a trial, with overlaid path data of the red and blue pixels, the pixels midpoint (centre between red and blue), the centre of mass, and the axis of cable connection. The lines represent the respective paths over a full 60 second trial.

2. to calculate the consistency of the readings (by calculating the standard deviations between peaks, saved as **Max peaks period std** (M_σ) [s] and **Min peaks period std** (N_σ) [s]).

The latter calculation is an important indicator variable, as large inconsistencies can flag irregular floater behaviour or a failure in signal peak detection.

Indeed, during the creation of the script large M_σ and N_σ values were found and were attributed to failures in signal peak detection. This was found to primarily lead to inaccurate response frequency readings. Therefore, a fast-fourier transform (fft) was implemented, which more successfully identifies the main frequencies of the response and their amplitudes. The limitation is that the dominant frequency may be of lower amplitude than the highest regular amplitude achieved by the floater, as it can combines several constructive frequencies. For this reason, the paper proceeds to use the peak-to-peak-obtained **Amplitude** measurement, and the fft-obtained **Dominant Frequency** (f_1) [Hz] measurement.

Third, the distance travelled per second, or simply **Velocity** (v) [m/s], in the Surge, Heave, and Pitch directions is calculated. The distance travelled can be correlated to work being done, and therefore power production when taken over time. It is a reliable performance

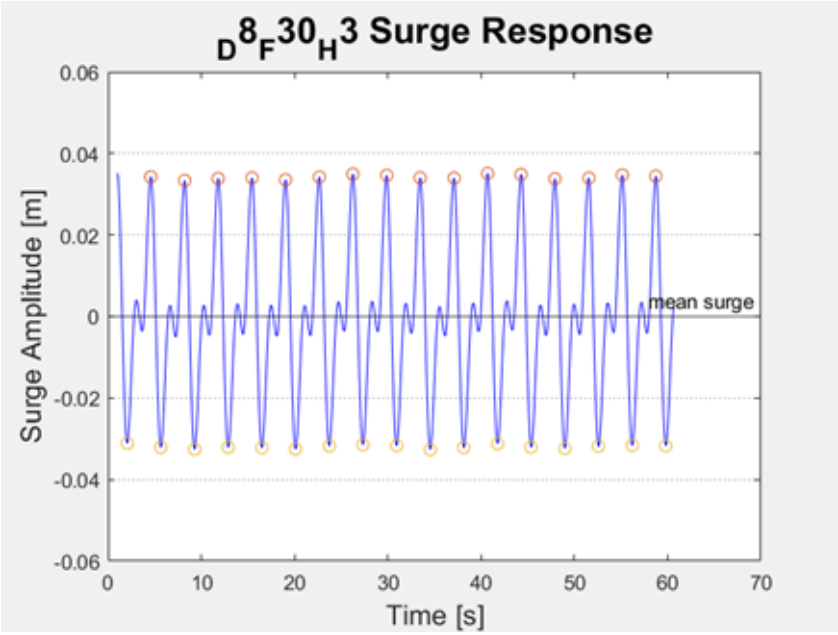

Figure 5.3: The surge response, measured at M_c. for the case: Draft index 8, Frequency index 30, trial 3. Maximum and minimum peaks are circled in red and orange respectively.

indicator as it accounts for the entire movement, rather than a single component like peak-to-peak-amplitude. One limitation is that it is highly correlated with the wave frequency. That is, a sub-optimal floater in increasingly rapid waves is likely to move increasingly rapidly itself, more rapidly, even, than an optimal floater in slower waves. The sub-optimal configuration, having covered more distance, will wrongly present itself as the superior option. Therefore comparisons of **Velocity** can only be made within groups under the same wave conditions. To allow for inter-group analysis, the **Velocity** data is nomalised with respect to **Wave Frequency**:

$$\text{Velocity per wave frequency} = v/W_f \tag{5.6}$$

Lastly, all of the calculated data is collated into two tables for analysis.

The following Table 5.1 identifies and describes all variables that were calculated during data processing. The number of variables referred to in this paper are kept minimal, but due to the complexity and similarity of the variables, readers may find it useful to refer to.

5.3 Data analysis

Data analysis is conducted using Microsoft Excel and Minitab. Firstly, the gathered data is validated, to ensure that the experiment has been executed correctly, and that all measurement systems worked adequately. This is done for the wave generator system, and

Category	Variable Name	Symbol	Unit	Description
Floater	Draft	D	[mm]	Mean height of the water line from the floaters' base at steady state
	Draft Index	D_i	[dmnl]	A number representing the draft value, used as an indexing element
	Cable Length	L	[m]	The mean length of the two mooring cables, measured from the base of the wave flume (including the length of the carabiner) to the floater connection point.
Waves	Wave Frequency	W_f	[Hz]	The number of peaks which pass a stationary point relative to the wave every second
	Wave Intensity	W_i	[dmnl]	The number given by the wave-generator, corresponding to its' rotational frequency. It is used as an indexing element, and as a rough indicator of relative wave intensity.
	Wave Height	W_h	[m]	The mean height of the waves in the trial, measured from bottom of trough to top of peak (peak-to-peak amplitude)
	Wave Period	P	[s]	The mean time span between wave peaks
	Wavefrequency/Cablelength ratio	W_f/L	[dmnl]	A ratio between wave frequency and cable length
Surge/ Heave/ Pitch/ Yaw/Sway	Amplitude	A	[m]	The mean peak-to-peak amplitude
	Max peaks period mean	$M_{\overline{x}}$	[s]	The mean time span between maximum-amplitude peaks
	Max peaks period std	M_σ	[s]	The standard deviation of the mean time between maximum-amplitude peaks
	Min peaks period mean	$N_{\overline{x}}$	[s]	The mean time span between minimum-amplitude peaks
	Min peaks period std	N_σ	[s]	The standard deviation of the mean time between minimum-amplitude peaks
	1st amplitude	A_1	[m]	The peak-to-peak amplitude of the dominant frequency identified by the fast-fourier transform
	2nd amplitude	A_2	[m]	The peak-to-peak amplitude of the second-most-dominant frequency identified by the fast-fourier transform
	Dominant Frequency	f_1	[Hz]	The frequency value of the dominant frequency identified by the fast-fourier transform
	2nd frequency	f_2	[Hz]	The frequency value of the second-most-dominant frequency identified by the fast-fourier transform
	2nd freq significance	q	[dmnl]	The ratio between the 2nd and 1st frequencies, indicating the proportional magnitude of the 2nd frequency to the 1st.
	Velocity	v	[m/s]	The mean velocity of the floater during the trial
	Velocity per Wave Frequency	v/W_f	[m/s/Hz]	The mean velocity of the floater during the trial, normalised by Wave Frequency (Wf)
	Harmonic number	n	[dmnl]	The factor by which Wf is multipied to get f1
Yaw/Sway	Marker distance change	Δd	[m]	The distance between the red and blue tracking markers.

Table 5.1: Table detailing the names, symbols, units, and descriptions of all variables calculated during data processing.

for the ultrasonic sensor readings. Next, the gathered data needs to be inspected and cleaned of any remaining anomalous readings, for both Surge and Heave data.

5.3.1 Equipment and Measurement Validation

In order to conclude that the wave data collected is valid, both the repeatability of the physical wave generator system (i.e. for an identical **Wave Intensity** setting, does it produce an acceptably similar wave condition?), and the repeatability of the ultrasonic measurement system (i.e. all things being equal, will the measurement system output acceptably similar data?) must first be validated.

Wave Generator

The repeatability of the wave generator system is currently unknown due to the lack of a live feedback measurement system during the experiment; the wave conditions were set solely according to the **Wave Intensity** display, and there was no additional indicator of wave conditions to inform the experimenter of whether or not the wave conditions were consistent in reality.

Ultrasonic sensor data

The resolution of measurement achievable via ultrasonic sensor is limited by its accuracy, which for this experiment was conservatively estimated to be about 1% of the measured

distance. At a distance of $0.24m$ from the water surface, the sensors were operated at a resolution of $0.01m$. In trials with the lowest **Wave Intensity**, the wave elevation would not vary more than $0.03m$, which is close to the sensing limit of the sensor. A plotted example of such readings can be seen in Figure 5.4; note the square nature of the readings, and the protracted, many-pointed peaks. Due to the low-resolution data, it follows that the the **Wave Height** and **Wave Frequency** data-points calculated from these readings are at risk of error, and require validation.

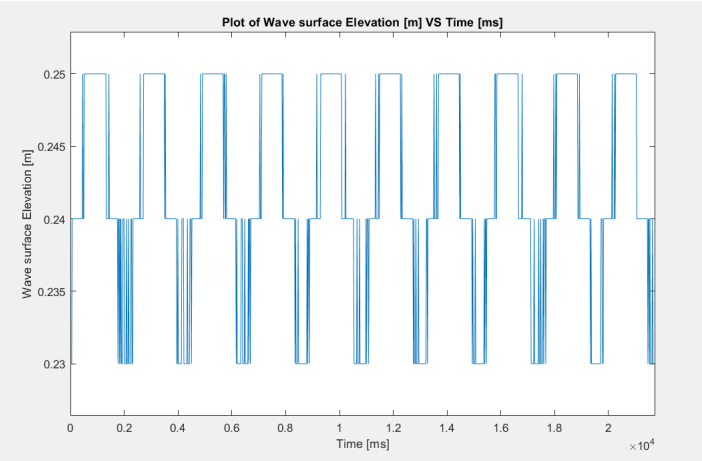

Figure 5.4: A plot of Wave surface Elevation (m) against Time (ms), for a ***Wave Intensity*** *setting of 20.*

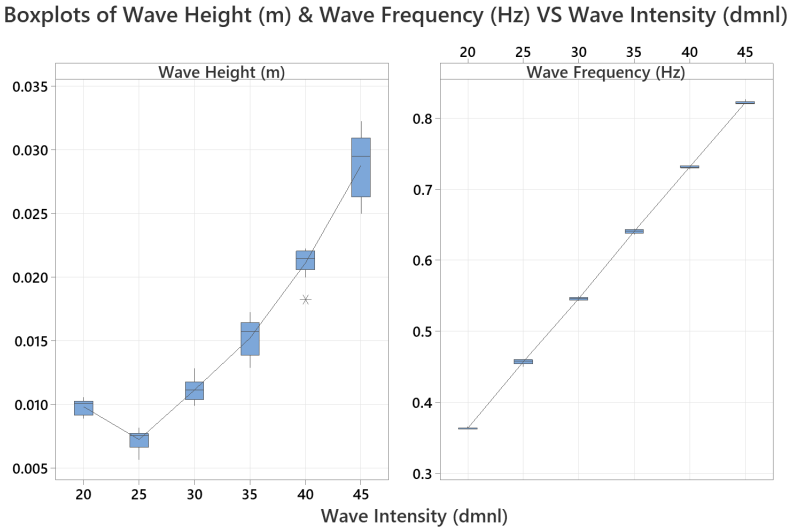

Figure 5.5: Boxplots of ***Wave Height*** *[m] (Left) and* ***Wave Frequency*** *[Hz] (Right) against* ***Wave Intensity*** *[dmnl].*

In Figure 5.5, the boxplot of **Wave Frequency** against **Wave Intensity** shows remarkable

consistency. The extremely tight groupings and perfectly linear progression are *only possible* when both the wave generator system and the frequency measurement system are functioning repeatably. Therefore, this plot proves the validity of both these systems. By performing a linear regression, an equation relating **Wave Intensity** (W_i) to **Wave Frequency** (W_f) can be found:

$$W_f = -0.002378 + 0.01833 W_i \tag{5.7}$$

In the boxplot on the left, a relatively large variation in **Wave Height** measurements in each group can be seen, as well as a non-linear trend with increasing **Wave Intensity**. This is unlikely to be the case in reality, since water waves in identical conditions, and with identical excitation, would be expected to propagate with the same amplitude. Furthermore, water waves excited with increasing energy are expected to possess greater amplitudes, within reasonable tolerances [Dingemans, 2000]. The uncharacteristic rise in **Wave Height** at $W_i = 20$ defies this principle.

Since neither the large variation nor the irregular trend can be attributed to real phenomena, it is concluded that the measurement system is unable to accurately measure **Wave Height**, thus making the data unusable. Only **Wave Frequency** data will be used for analysis purposes.

5.3.2 Data Cleaning

The colour-tracking system used to track the location of the centre-of-mass of the floater is ideal for tracking movement in the 2-dimensional case, where the floater moves only along the plane normal to the filming direction (the "Normal" plane), exercising only 3 degrees of freedom: Surge, Heave and Pitch motion. However, it is susceptible to false measurements when other degrees of freedom are involved. The most prominent and problematic modes of interference for this study are:

- Roll interference, causing false heave measurements due to the front face of the floater rotating up and down, whilst the centre of mass remains stationary.
- Yaw interference, causing the front face to rotate left or right from the perspective of the camera, whilst the centre of mass remains stationary.

The schematic in Figure 5.6 provides a visual explanation of how these measurement errors occur. Data analysis tools are employed to identify where these measurement errors occurred, and to eliminate them.

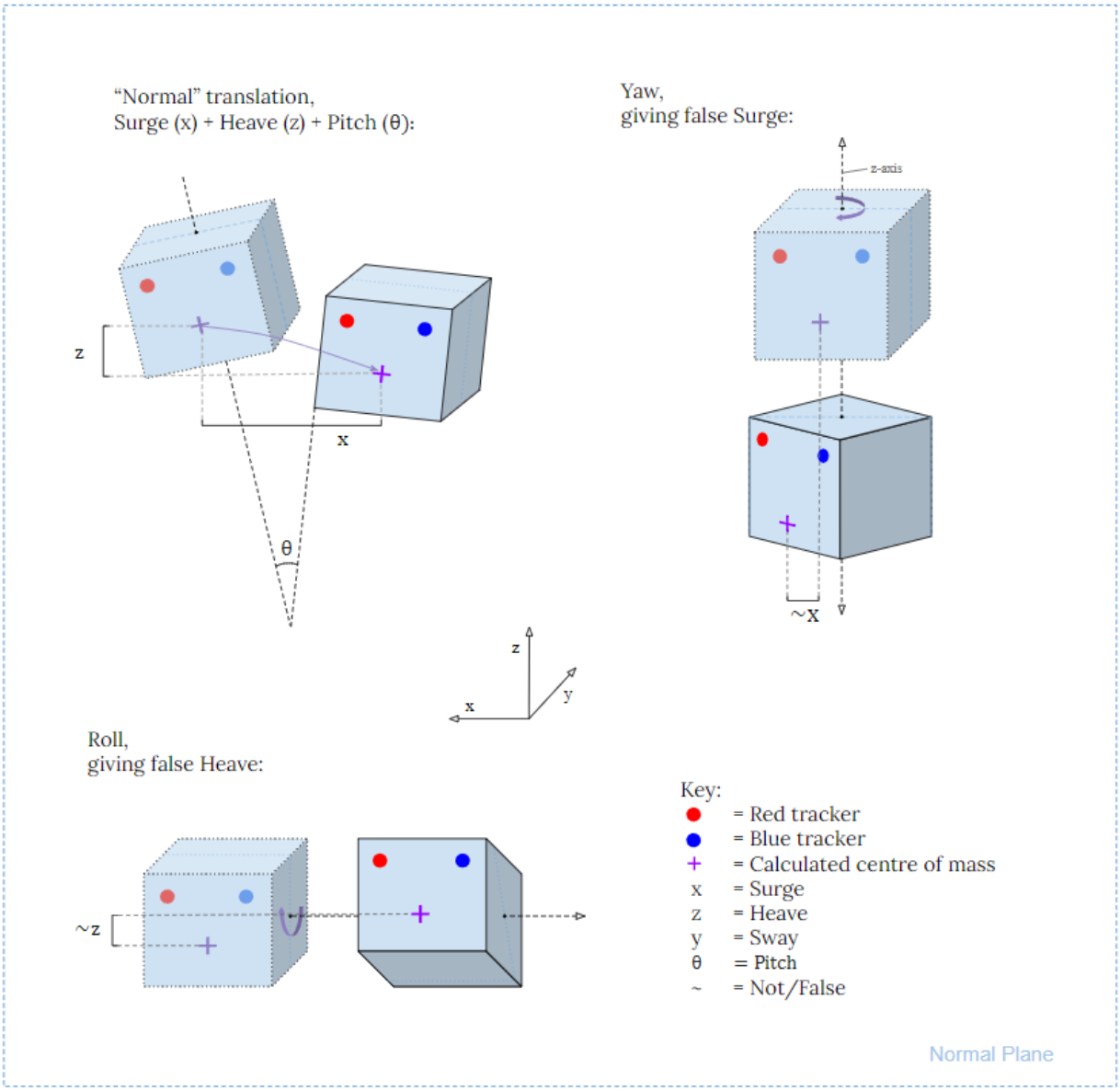

Figure 5.6: Schematic detailing "Normal" translation (translation in 3 deg. of freedom) and how it is measured, as well as Yaw and Roll motion, and how this motion results in false Surge/Heave measurements, respectively.)

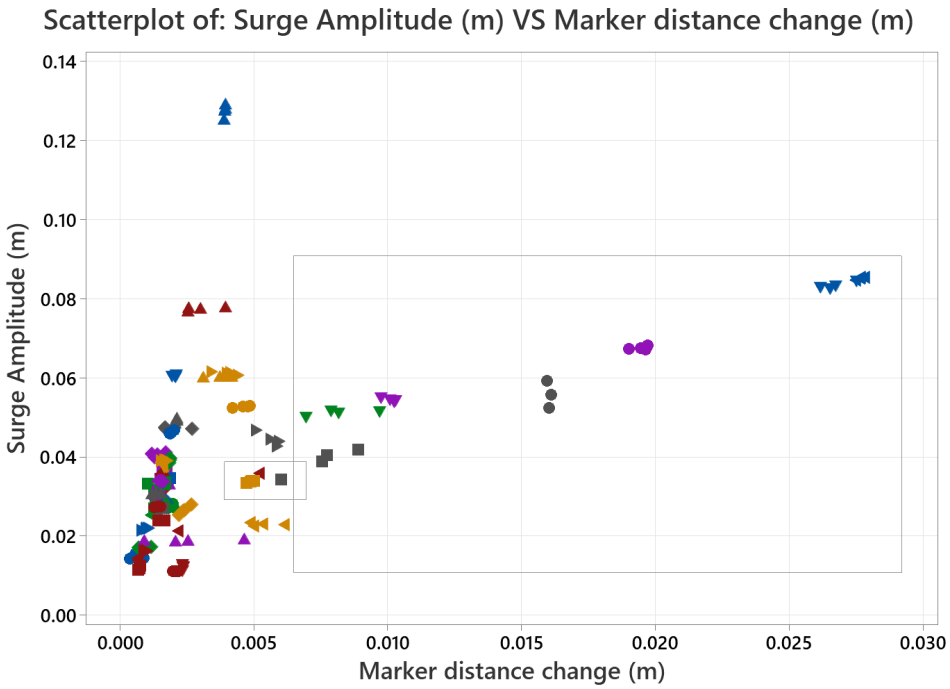

Figure 5.7: Scatterplot of ***Surge Amplitude*** *against* ***Marker distance change****, grouped by* ***Draft-Wave Intensity*** *pairs. The boxes indicate the data points that are deemed to have unreliable Surge data, due to an interfering component of Yaw.*

Surge data

By plotting Surge **Amplitude** against **Marker distance change** (Δd), the data points with large Δd components can be easily identified[1] (see Figure 5.7). The video file for each data point was reviewed and, if significant and interfering[2] Yaw was observed, the Surge data was removed from the data set. For a detailed view of which items were removed, refer to Appendix Figure 3.

Heave data

Heave detection is susceptible to Roll interference. Unfortunately, the colour-tracking system is not capable of detecting Roll to a high degree of accuracy, so the same approach cannot be used as with Surge data. Instead, the video data is filtered through manually, and any trials with significant Roll behaviour are eliminated from the data set. Refer to Appendix Figure 4 for details on which files were removed.

[1]It may be interesting to note that a somewhat positive relationship can be seen between Δd - which corresponds roughly to Yaw - and Surge **Amplitudes**, but this relationship only exists due to the Yaw interference in Surge measurement; it does not reflect reality.

[2]The Yaw measurement is itself susceptible to Roll and Sway interference, both of which do not interfere with Surge measurement. This is why some data points with relatively high Yaw **Amplitude** were retained - because the measured Yaw reflects either Roll or Sway, and the Surge measurement was deemed valid.

6 RESULTS AND DISCUSSION

In this experiment, the independent variables are the **Cable length** (L) and **Wave Intensity** (W_i) (which encompasses both **Wave Frequency** (W_f) and **Wave Height** (W_h)). The dependent variables are the Surge or Heave **Amplitudes** (A).

The current working hypothesis is that **Cable length** is an influencing parameter upon the fundamental frequency of a moored floater, and can thereby be used as a tuning parameter to achieve resonance with surrounding wave conditions, to maximise the Surge **Amplitude** (A) response. For brevity, this hypothesis will be referred to as the **Cable length-Wave Intensity** or L/W_i resonance-pair hypothesis. In this section, results that either support or oppose the hypothesis are discussed.

The first data to be investigated, in section 6.1, are how the Surge and Heave **Amplitudes** change with **Cable length** for wave conditions of increasing intensity (see Figure 6.1). Then, in section 6.2, observations about the harmonic frequency responses of the floater in the Surge direction are noted.

6.1 Amplitude Response

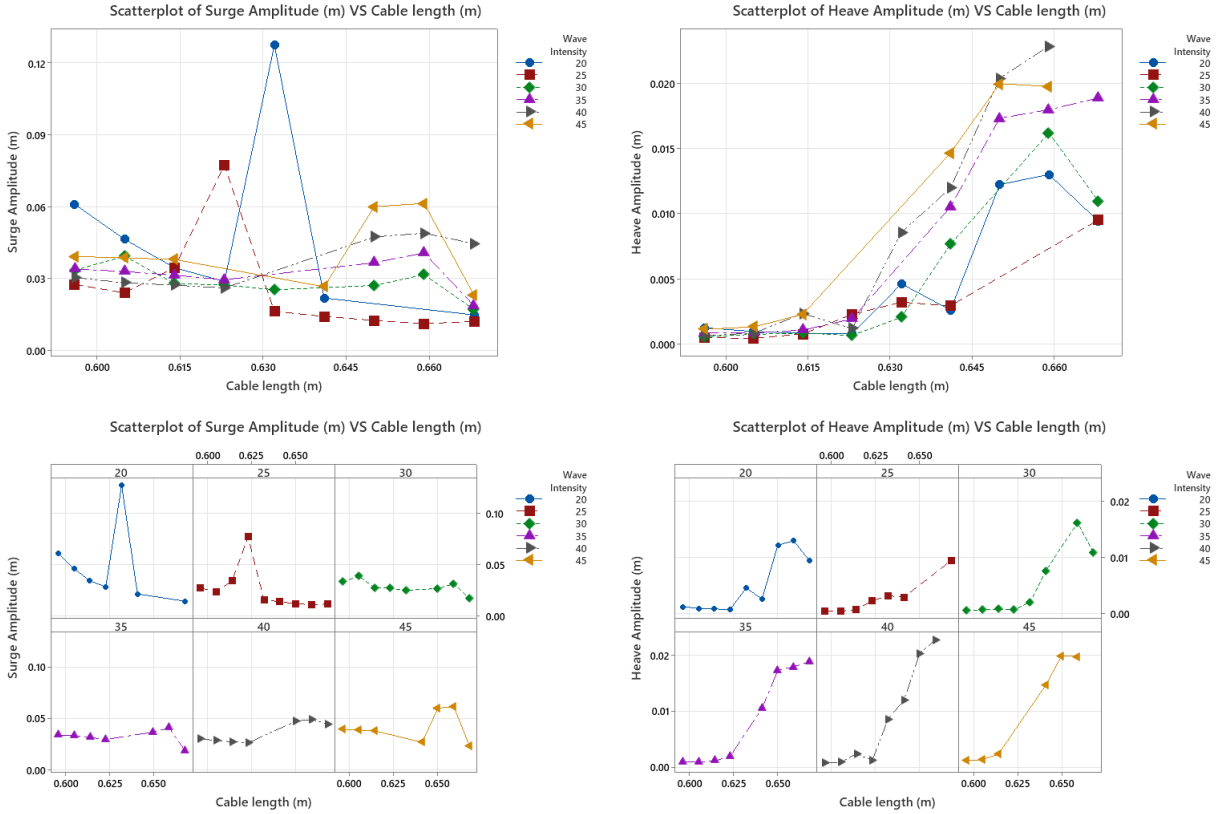

*Figure 6.1: Scatterplots of the **Amplitude** responses of the moored floater for increasing **Cable length**, grouped by wave conditions of increasing **Wave Intensity**. a) (Top left) Surge Amplitude response, b) (Top right) Heave Amplitude response, c) (Bottom left) Surge Amplitude response split by Wave Intensity groups into panels, and d) (Bottom right) Heave Amplitude response split by Wave Intensity groups into panels.*

Cable length [m]	0.596	0.605	0.614	0.623	0.632	0.641	0.65	0.659	0.668
Draft [mm]	150	140	130	120	110	100	90	80	70
Optimal Wave Intensity [dmnl]	20	20	45	25	20	45	45	45	40
Optimal Wave Frequency [Hz]	0.364	0.362	0.821	0.461	0.363	0.821	0.819	0.827	0.734
Optimal Wave Period [s]	2.745	2.761	1.218	2.171	2.755	1.218	1.220	1.210	1.363

*Table 6.1: Tabulated data from Figure 6.1(a), detailing the **Draft**, optimal **Wave Intensity**, optimal **Wave Frequency** and optimal **Wave Period**for the highest-amplitude data points for each **Cable length**. Green columns indicate suspected resonant pairs.*

6.1.1 Surge Amplitude

Figure 6.1(a) shows that most **Cable length** values correspond to a particular **Wave Intensity** which maximises the Surge **Amplitude** response. This indicates that mooring-cable length is a significantly influencing parameter for the Surge amplitude response of a moored floater, and supports the L/W_i resonance-pair hypothesis.

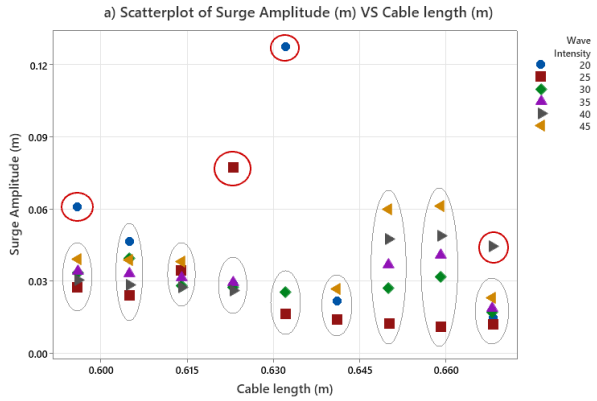

Figure 6.2: This is Figure 6.1(a), but with grey ellipses to indicate groupings, and red circles to indicate the outliers.

The grouping of the data in Figure 6.1(a) is of interest. Figure 6.2 on the left displays this grouping clearly. Within grey ellipses lie closely-grouped or evenly-spaced data points, and within red circled lie distant outliers: one per group at cable lengths of 0.596m, 0.623m, 0.632m, and 0.668m. This indicates that, for any given **Cable length**, the majority of wave conditions will produce similar Surge responses, but under *particular* wave conditions the system will produce an abnormally large Surge response. The extremity of the outliers suggests that, at those **Cable length-Wave Intensity** pairs, an optimising resonance was achieved. This observation supports the L/W_i resonance-pair hypothesis.

Furthermore, only 4 out of 9 cable lengths contain outliers, and all other observations are tightly grouped. This infrequency and distribution of resonant responses is consistent with mass-spring-damper theory; the moored floater acts as an oscillating body with little damping, and therefore has a sharp resonance peak [Cross and Plunkett, 2014]. This, too, supports the L/W_i resonance-pair hypothesis.

The final observation of interest is that: for different cable lengths, the spread of amplitudes of the suspected non-resonant responses varies. This can be seen in Figure 6.2 as grey ellipses of different heights. No causal explanation for this phenomenon could be found. The spread appears to be unrelated to the relative magnitude of the resonant response.

In Figure 6.1(c) the progression of Surge **Amplitude** with respect to changing **Cable length** can be clearly seen panel by panel for each **Wave Intensity**. Going from top left to bottom right: the panels for $W_i = 20, 25$ contain solitary, extreme peaks. $W_i = 30, 35, 40$ have much less prominent peaks, and 45 contains two peaks of very similar magnitude next to each other. The lack of clear resonance peaks in the later panels may be evidence against the L/W_i resonance-pair hypothesis.

However, it is also possible that the resonant **Cable length** pair for **Wave Intensities** 30, 35, and 40 is either a) not within the testing range, b) in between tested values, or c) the resonant amplitude is shown, but it is less extreme than for the cases $W_i = 20, 25$. The visible double-peak in the case $W_i = 45$ suggests that a resonant peak lies in between

$L = 0.650, 0.659$ meters.
Unfortunately, the collected data is currently insufficient in both range and resolution to prove or disprove either claim.

6.1.2 Heave Amplitude

The floater Heave response, plotted in Figure 6.1(b), displays an overall positive trend. This resembles the same trend obtained by [Asiikkis et al., 2023] (See Appendix Figure 5) in their theoretical study. This positive trend was central to the authors' hypothesis that there exists an inverse relationship between Heave and Surge responses, due to available energy being allocated to one direction at the expense of the other. However, Figure 6.3 shows that no such relationship exists. Furthermore, no direct nor indirect statistically-significant explanatory relationships could be found between Heave and Surge **Amplitudes** in this research.
Despite this, insights obtained in this study have led to a near-comprehensive understanding of the Heave **Amplitude** response: the observed trend in behaviour is believed to be directly linked to the physical limitations imposed upon the floater by the length of the mooring cable, and by the elevation of the water line relative to the natural draft line. The extent of the limitation is broken down into three distinct zones: "too-tight", "loose", and "too-loose", which are highlighted in Figures 6.4(a) and 6.4(b).
In order to develop an intuitive understanding of the zones and why certain Heave behaviour can be attributed to them, the zones are sequentially defined and explained. The schematic in Figure 6.5 has been developed as a visual aid.

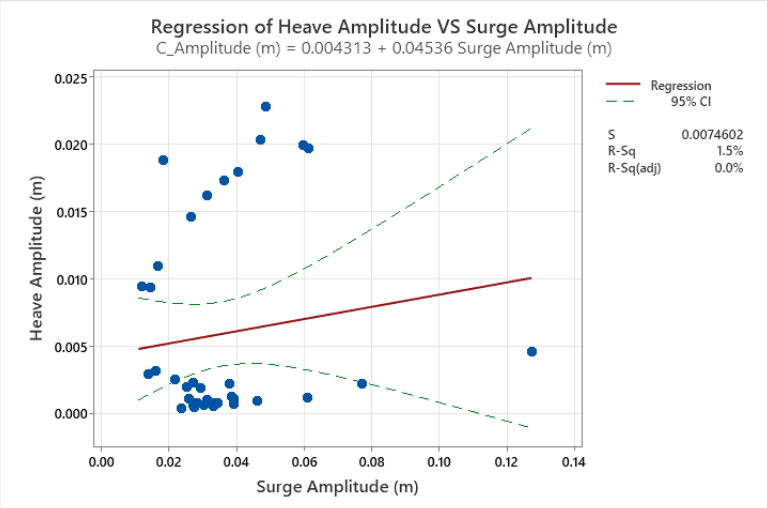

*Figure 6.3: Scatterplot of Heave **Amplitude** against Surge **Amplitude**, with a linear regression (shown in solid red) and 95% confidence intervals (shown in dotted green). On the right are statistical measures: S indicates the standard error. R-sq indicates R^2. R-sq(adj) indicates the R^2-adjusted value, which is 0.0%, showing that Surge **Amplitude** has no predictive power over Heave **Amplitude**.*

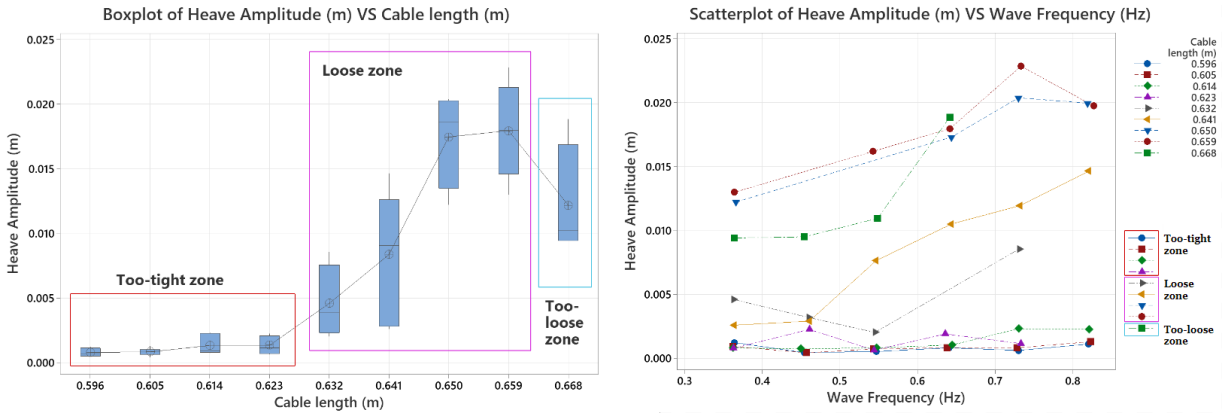

Figure 6.4: (Left): a) A Boxplot of Heave ***Amplitude*** *against* ***Cable length****, with coloured boxes indicating the delimited zones (from left to right: Red-"Too-tight zone", Pink-"Loose zone", Cyan-"Too-loose zone"). The line connecting the boxes indicates the mean. Note that this plot is a boxplot representation of the data visible in Figure 6.1(b). (Right): b) Scatterplot of Heave* ***Amplitude*** *against* ***Wave Frequency****, grouped by* ***Cable lengths****. In the bottom left, a key indicates which cable lengths belong to which zones. The zones are consistent between the plots.*

1. The "too-tight zone" at $L = 0.596, 0.605, 0.614$, and 0.623 meters, characterised by a narrow spread of data with extremely small A.
2. The "loose zone" at $L = 0.632, 0.641, 0.650$, and 0.659 meters, characterised by a larger spread of data, with a steeply - and then gently - increasing mean A.
3. The "too-loose zone" at $L = 0.668$m, showing a drop in mean A.

1) For the shortest **Cable lengths** in the "too tight" zone, the floater is held firmly in place vertically by the high cable tension pulling downwards against the equal and opposing buoyant force pulling upwards. The polypropylene cable is stiff, and does not allow any further Heave motion once taught, regardless of the **Wave Intensity**. This is why very little Heave **Amplitude**, or change in Heave **Amplitude** with greater **Wave Frequency**, can be observed in this zone.

2) In the "loose" zone, the mooring cables are increasingly long enough to allow for Heave movement, which explains the mean increase in A. Furthermore, Figure 6.4(b) shows that for individual **Cable lengths** in the "loose zone", the Heave A increases with increasing **Wave frequency**. This occurs because Heave is limited in the positive direction by the cable length, but can decrease as low as the trough of the wave. Deeper troughs are seen in waves of higher **Wave height**, and there is a positive relationship between W_h and W_f (Equation 5.7), explaining why Heave A increases with **Wave Intensity** in this zone.
At $L = 0.659$m, the last cable length in the "loose" zone, the **Draft** $= 80$mm, which is

slightly more than the natural **Draft** of the floater (78mm). This means that there is a very slight cable tension pulling the floater down, keeping it steady, but it is otherwise the most free to move vertically out of all **Cable lengths** in the zone, and it indeed possesses the greatest mean Heave A.

3) At the longest **Cable length**, $L = 0.668$m, the **Draft** remains at 80mm, and there are 9mm of loose cable. Therefore theoretically, it could exhibit a larger Heave A than the shorter cable lengths. Figure 6.4(b) shows that this only occurs in 1/4 measured cases. It is currently unclear why this is. It should be noted, however, that the lack of cable tension changes the dynamics of the moored floater considerably; the first two zones impose a direct physical limitation on the Heave motion of the floater, but in the third zone the magnitude of the Heave response is dependent on unknown factors. Therefore the "too-loose" zone may be treatable as separate from the rest of the collected Heave data.

This analysis provides a complete understanding of the trends of Heave **Amplitude** response observed in the cases $L < 0.668$m, or where **Draft** is below the natural draft of the floater. It is shown that there is a range of **Cable lengths** (the "loose" zone) for which Heave **Amplitude** increases consistently with both **Cable length** and **Wave Frequency**. The approximate optimal value of **Cable length** lies at

$$L' = L_D - s \tag{6.1}$$

where L' is the optimal **Cable length**, and L_D is the **Cable length** at which **Draft** is equal to the natural draft, and s is some small number.

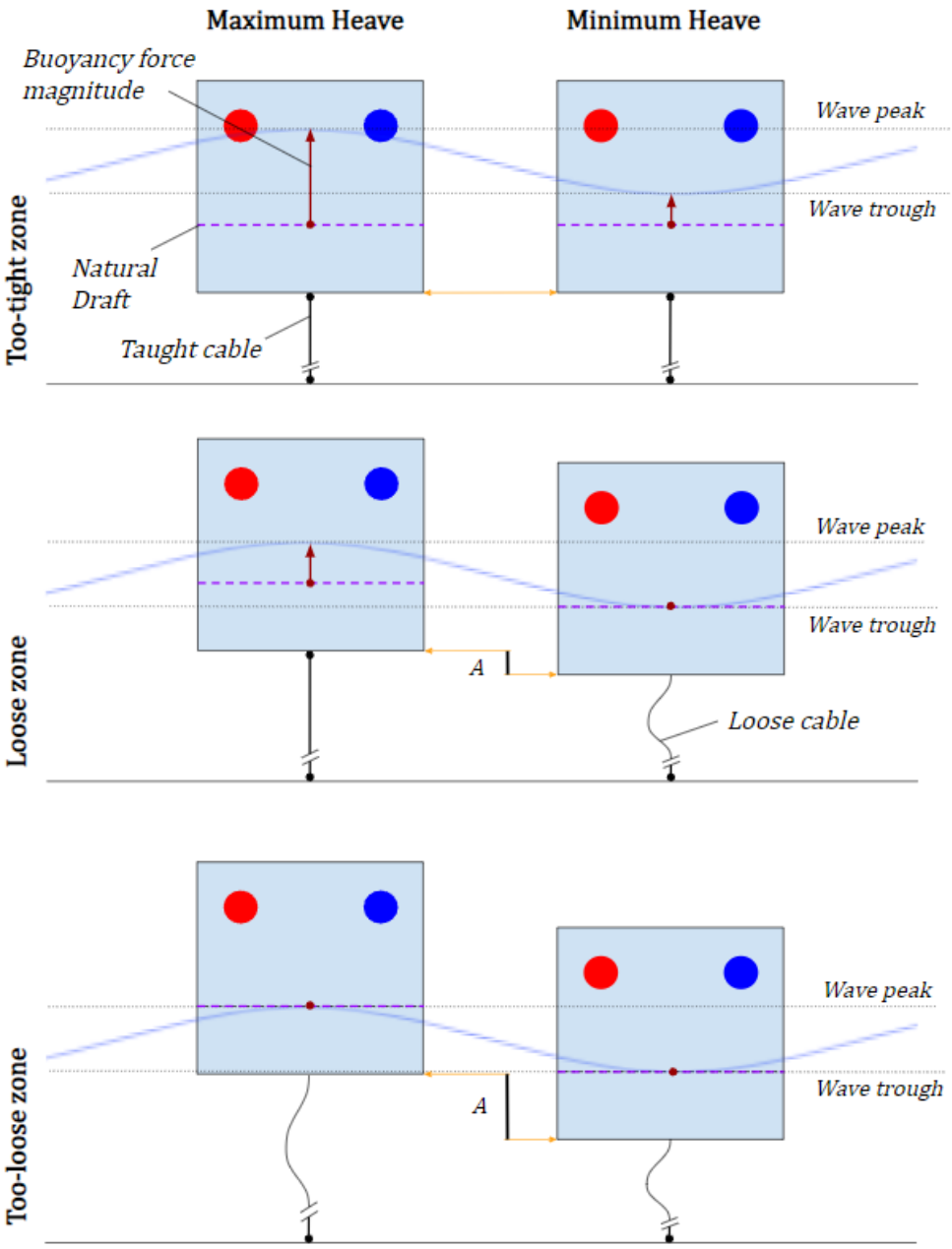

Figure 6.5: Schematic of the moored floater at maximum and minimum Heave positions, under the three zone conditions: 1) "too-tight", 2) "loose", and 3) "too-loose".

6.2 Surge Frequency Response

By plotting the Surge **Dominant Frequency** against **Wave Frequency** in Figure 6.6, it is clear that the floater responds in harmonic frequencies. This is not unusual as a natural phenomenon. From this plot, the **Harmonic Numbers** n are calculated. It is found that the floater responds in harmonic frequencies with harmonic number $n = 0.5, 1$. The bubbles are sized by Surge **Amplitude**; no obvious relationship can be seen with respect to either **Wave Frequency** or **Harmonic Number**.

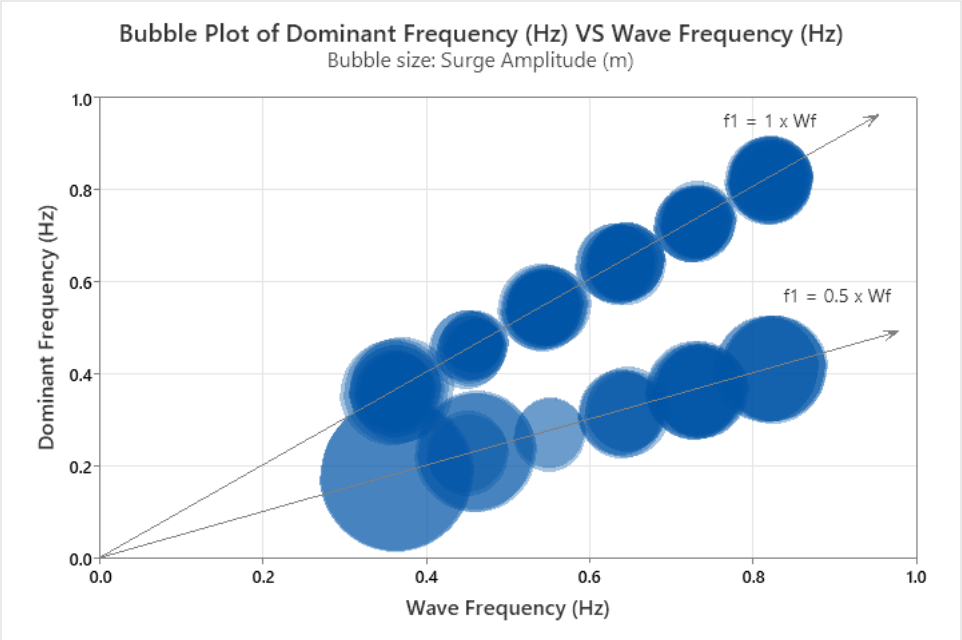

Figure 6.6: Scatterplot of Surge ***Dominant Frequency*** *(f_1) against* ***Wave Frequency*** *(W_f), with bubbles sized by Surge* ***Amplitude****. Each bubble represents one trial. Reference lines are labelled with equations $f_1 = n * W_f$, with n being the* ***Harmonic Number****.*

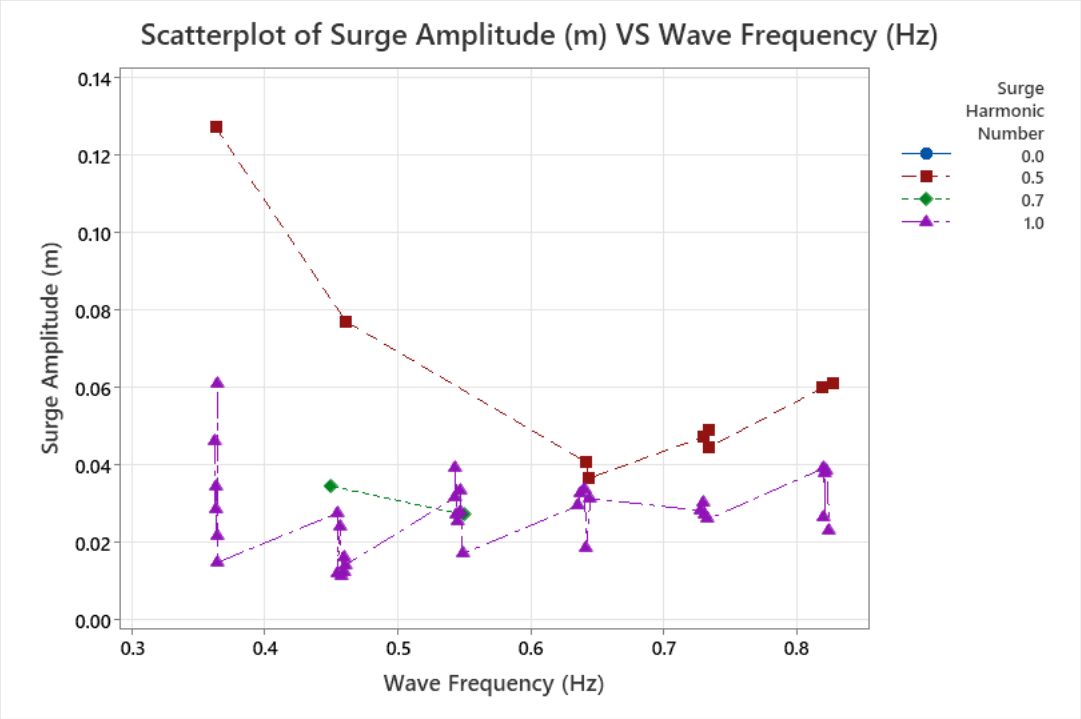

Figure 6.7: Scatterplot of Surge ***Amplitude*** *(A) against* ***Wave Frequency*** *(W_f), grouped by Surge* ***Harmonic Number*** *(n)*

Figure 6.7 displays Surge **Amplitude** against **Wave Frequency**, grouped by **Harmonic Number**. Within every **Wave Frequency** group, responses of **Surge Harmonic Number** $n = 1$ and 0.5 can be seen. Most notably, responses with $n = 0.5$ are *consistently* the highest in **Amplitude**. This implies that **Surge Harmonic Number** is an optimising variable for Surge **Amplitude**, where a moored floater produces the most optimal responses when it oscillates at half the frequency of the incident waves.
Furthermore, considering that within each **Wave Frequency** group the only independent variable is **Cable length**, the change in **Harmonic Number** can be attributed to the change in **Cable length**. This proves that a direct, causal relationship exists between **Cable length** and the **Harmonic Number**, which in turn has been shown to maximise Surge **Amplitude** at a specific harmonic frequency. The implication of this finding is that the L/W_i resonance-pair hypothesis is proven to be true, but with one caveat: that is, that the optimal harmonic condition of the floater is not the expected resonant frequency, but instead half the resonant frequency.

To summarise:
The research so far has proven that, within this experiment, the mooring **Cable length** is found to be a directly influential parameter upon the fundamental frequency of the model floater. It can thereby be used as a tuning parameter to achieve varying harmonic

frequency responses to the incident waves. Moreover, a harmonic frequency of $n = 0.5$ has been found to consistently produce maximal Surge **Amplitude** responses. Therefore, the mooring **Cable length** can be used as a tuning parameter to achieve a maximal Surge response in the floater.
These findings support the aforementioned findings and hypothesis laid out by [Asiikkis et al., 2023]. This serves to further reinforce the idea that a Surge-based PA-WEC may be controllable via its mooring cable length, which may in turn be an advantageous characteristic for future PA-WEC design.

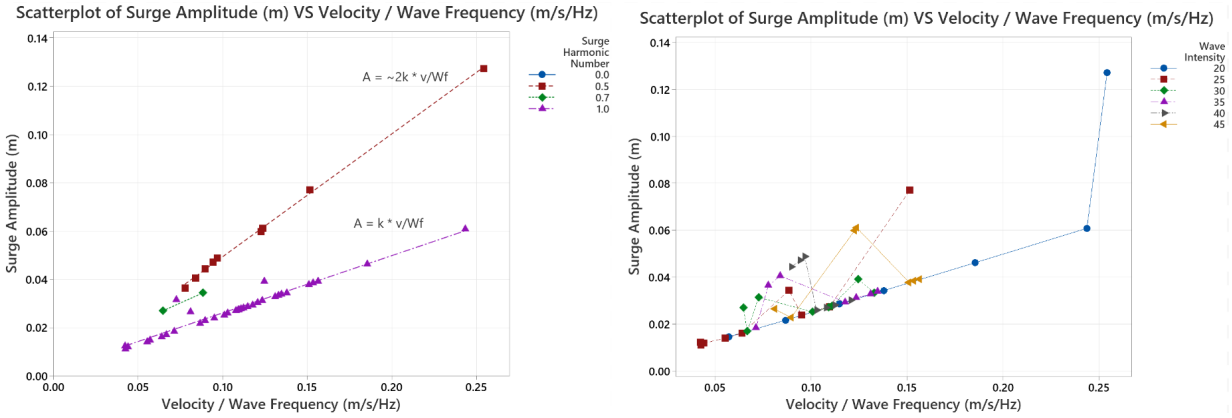

Figure 6.8: (Left): a) Scatterplot of Surge ***Amplitude*** *(A) against Surge* ***Velocity/Wave Frequency*** *(v/W_f), grouped by Surge* ***Harmonic Number*** *(n). The groups have regression lines and approximate algebraic equations describing them.This symbol means 'approximately': ˜. Let k be some positive real constant. (Right): b) The same data as in (a), instead grouped by* ***Wave Intensity****.*

In Figure 6.8(a) an interesting relationship between Surge **Amplitude** (A), Surge **Velocity / Wave Frequency** (v/W_f), and Surge **Harmonic Number** (n) is observed. Surge A increases linearly with v/W_f within harmonic groups. This is to be logically expected in ideal conditions: if, for a given **Wave Frequency** and **Harmonic Number**, an oscillating body increases the amplitude of its oscillations, the velocity must also increase. However, the near-perfect linearity of the data is surprising, and shows that a very strong relationship exists between Surge A, v/W_f and n.
Linear regressions were performed on the values at $n = 0.5$ and $n = 1.0$, to obtain linear mathematical expressions of the trends:

$$\begin{aligned} n = 0.5 : A &= -0.001500 + 0.5085 \left(\frac{v}{W_f} \right) \\ n = 1.0 : A &= 0.002379 + 0.2370 \left(\frac{v}{W_f} \right) \end{aligned} \tag{6.2}$$

Both Y-intercepts are near zero, and the coefficient for $n = 1$ is 2.145 times the coefficient

for $n = 0.5$. Let the coefficient be called k. Extrapolating the data, the following equation can be found relating n and k:

$$k = 0.63875 - 0.2715n \tag{6.3}$$

Using this equation, the expected slope of the line relating Surge A and v/W_f at a specific **Harmonic Number** n can be known. Then, a mathematical model can be built which predicts the *theoretically possible* A-v/W_f pair locations. This could be useful in practice if, for example, the efficiency of a PTO is dependent upon the oscillation velocity of the floater, and it is therefore an optimising parameter to consider alongside the Surge **Amplitude**. Note that the equation is extrapolated from only two data trends, and the true governing equation may be far more complex. It serves only as a rough indication of the relationship between n and k in this experiment, and as an illustration of how a predictive model could theoretically be created.

The plot in Figure 6.8(b) shows how changing **Cable length** alone influences the **Amplitude** response: in each W_i group, the Surge response 'jumps' between harmonic frequencies, and thereby between the harmonic slopes, as **Cable length** is changed.
It has previously been proven that there is a causal relationship between **Cable length**, **Harmonic Number**, and Surge **Amplitude**. The analysis of Figure 6.8(a) illuminated a fourth dependent variable, **Velocity / Wave Frequency**. Whilst the equations governing those relationships remain unknown, Figure 6.8(b), and equations 6.2 and 6.2 serve to define them to some extent.

7 LIMITATIONS

Internal Limitations
Major limitations of the scope and results of this research stem from the inherent limitations set by the measurement systems used in the experimental design.

- Despite best efforts to minimise behaviour outside of the desired 3 degrees of freedom, and cleaning the data of any suspected false measurements where it did occur, the tracking system used in this experiment is reductive and susceptible to error, as explained in subsection 5.3.2. Due to this inability to precisely and accurately measure real behaviour, all results achieved are subject to scrutiny and the analysis is limited to studying behavioural trends, rather than specific data. Furthermore, Heave data had to be cleaned manually, due to the systems inability to distinguish Roll from Heave behaviour. While this proved to be adequate for the purpose of this research, future research may wish to employ an improved tracking system in order to avoid measurement error, human error in data cleaning, and to gain a more comprehensive description of the floater kinematics.

- Subsection 5.2.3 concerns itself in part with the justification of the 'tracking point' being located in-line with the centre of mass of the floater. It is important to note, however, that other tracking points may have also been adequate, or even superior, and may have produced entirely different results. The visible difference between the 'centre of mass path' and 'cable connection path' in Figure 5.2 illustrates this. The implications is that the results of this study stem from this near-arbitrary choice of tracking point, and are influenced by it to an unknown degree.
- Measurement validation in Subsection 5.3.1 revealed that **Wave Height** measurements were unreliable, and therefore unusable. The root cause of this is thought to be the low resolution of measurement achieved by the ultrasonic sensors. This excluded **Wave Height** from analysis, thus limiting the scope.
- The results are limited only to the range and resolution of **Cable lengths** and **Wave Intensities** measured, and extrapolations of this data cannot be made with certainty. For example, the conclusion that $n = 0.5$ is consistently optimal is limited to the measured values.
- The experimental setup was not capable of measuring wave length, wave speed, or the phase response of the floater. These omissions also limited the scope of the analysis and research as a whole.

External Limitations

This study is exploratory in nature, and as such it does not concern itself deeply with the external validity of its methodology or findings. Nontheless, the elements of the study which most limit the external validity are listed.

- The design requirements of the moored floater were not based on realism. Little effort was taken to design it to-scale, with respect to the incident waves, or the floater-size to cable-length ratio. Furthermore, a PTO was not included. These factors were deemed outside the scope of the research.
- The mooring configuration involved semi-loose and stiff cables. This is not typical of functional PA-WECs, because of the 'cable snap' that occurs when they suddenly become taut, exerting unsustainably large forces on the cables and connection points. Damping is usually implemented in the system via catenary lines, elastic mooring lines, or mechanical damping from the PTO, which changes the hydrodynamics of the entire system. In particular, this limits the explanation found in this paper for trends in Heave motion.
- The experiment is reductive in its imitation of realism: the floater was subjected to a single repeated wave travelling in one dimension, with no wind. Under more realistic conditions of multiple-frequency waves, incident at random directions and under wind forces, the hydrodynamics of the system may change substantially.

The implication of each point is that the findings of this study may not be applicable to

real PA-WECs.

8 FUTURE RESEARCH

- Although the existence of a causal relationship between **Cable length** and Surge **Amplitude** was established, and some progress was made in deciphering the nature of the relationship via the **Harmonic Number** and **Velocity / Wave Frequency**, the exact equations governing the relationship remain unknown. Obtaining this knowledge is necessary in order to be able to effectively tune a Surge-based PA-WECs response via **Cable length**. Therefore, this is recommended as an area which would benefit from further research.
- Moreover, equation 6.2 in Section 6.2 describes a relationship between **Harmonic Number** n and coefficient k. As it stands, the equation is limited in accuracy due to the lack of data points. However, the results of this research suggest that a more developed understanding of the equations governing these interactions would be of value.
- The results of the current experimental setup can be greatly enhanced by reproducing the experiment with greater range and resolution for both **Cable length** and **Wave Intensity**.
- Valuable further research could be conducted by exploiting the built-in modularity of the floater. The experimental conditions can be varied in terms of the mass of the floater, the mass distribution, density, the cable stiffness, cable weight, number of cables, cable constellation, et cetera.
- The internal and external validity of the experiment can be improved by addressing the limitations noted in Section 7.
- A detailed literature review into the current 'state of the art' of Surge-based WECs could be extremely valuable for any further research in this field. Principles of Surge wave energy capture from other types of WECs could be applicable to a PA-WEC.

9 CONCLUSION

This study aimed to:

(a) Develop a proficient physical PA-WEC model and measurement system, within certain spatial and monetary limitations. Then use this system to effectively study the kinematic response of the model under varying mooring-cable-length and wave conditions.

(b) Identify behavioural trends of the model in the Surge direction, and, to a lesser extent, the Heave direction.

(c) Determine the extent to which the empirical results support or oppose the findings of the theoretical research in [Asiikkis et al., 2023].

First, pilot testing was performed using a limited experimental setup (Section 3). The problems and subsequent design requirements were identified. Then, in accordance with the design requirements, a proficient physical model and measurement system were created and implemented (Section 4). Using the completed experimental setup, the moored floater was subjected to a series of trials which tested for 6 **Wave Intensities** across 9 **Cable lengths**, with each pair conducted 3 times. The floater kinematics were recorded using a video camera, and the surface elevation of the water was recorded using an ultrasonic sensor (Section 5.1). The raw data was then processed in stages using MATLAB scripts, which measured and analysed the movement of the floater in 3 degrees of freedom: Surge, Heave, and Pitch, as well as an indicator of Yaw/Sway. The final script collated key performance and useful indicator data into a large table for analysis (Section 5.2). Then, the equipment and measurement systems were checked for bias and measurement error, and untrustworthy observations were discarded. The kinematic measurements were also cleaned of observations made invalid by movement in un-measurable degrees of freedom (Section 5.3). Transferring the cleaned and validated observations into Minitab, data analysis could be conducted, the results of which are discussed in detail in Section 6, and summarised below.

Primarily, it was found that **Cable length** is causally linked to the **Surge Harmonic Number**, which in turn tends to maximise Surge **Amplitude** at $n = 0.5$. Therefore, **Cable length** was proven to be an effective tuning parameter for the optimisation of Surge behaviour, in the case that maximal Surge **Amplitude** is the desirable state. This result directly supports the findings and hypothesis laid out by [Asiikkis et al., 2023], and reinforces the idea that Surge-based PA-WEC systems are worthy of further research, due to the potential advantages they may possess over Heave-based systems in terms of

optimisation control.
This research was unable to discover the specific equations governing the relationship between **Cable length** and Surge **Amplitude**.

Moreover, a linear relationship was found between Surge **Amplitude** and **Velocity / Wave Frequency** within individual harmonic groups. Approximate mathematical expressions governing the relationship were found. Though currently limited, the existence and simplicity of the expressions suggests that a predictive mathematical model could be developed, and the potential applications of such a model were discussed.

Contrary to the theoretical results, which suggested an inverse relationship between Surge and Heave **Amplitudes** due to limited energy allocation between them, no correlation was found between Surge **Amplitude** and Heave **Amplitude**.
However, a comprehensive intuitive explanation of floater behaviour in the Heave direction was developed. In short, Heave **Amplitude** was found to primarily be determined by the physical constraints imposed upon it by the length of the mooring cable (limiting positive Heave) and the buoyant force (limiting negative Heave). The optimal **Cable length** was found to be the length for which the **Draft** of the floater is slightly greater (2mm) than the natural **Draft**. These results may find application in Heave-based PA-WEC designs with stiff and loose mooring systems, or in Surge-based designs which wish to limit Heave motion.

This paper has found and explained several interesting behavioural trends found in a moored floater model in the Surge and Heave directions. Notably, it has confirmed the hypothesis that **Cable length** *can* be used as a tuning parameter to achieve optimal Surge **Amplitude**, which reinforces the prospect of designing a Surge-based PA-WEC using a cable-length-based response control system. Whilst the prospect's feasibility requires further research to assess, the author of this paper believes that results obtained here may serve as a fundamental stepping stone on the road towards developing novel renewable energy harvesting systems.

References

[WEC, 2021] (2021).

[Asiikkis et al., 2023] Asiikkis, A., Grigoriadis, D., and Vakis, A. (2023). Maximizing the surge amplitude of a floater through an adaptable mooring tightening technique. In *Proceedings of the European Wave and Tidal Energy Conference*, volume 15.

[Bacelli et al., 2019] Bacelli, G., Spencer, S. J., Patterson, D. C., and Coe, R. G. (2019). Wave tank and bench-top control testing of a wave energy converter. *Applied Ocean Research*, 86:351–366.

[Bechlenberg et al., 2023] Bechlenberg, A., Wei, Y., Jayawardhana, B., and Vakis, A. (2023). Analysing the influence of power take-off adaptability on the power extraction of dense wave energy converter arrays. *Renewable Energy*, 211:1–12.

[Cross and Plunkett, 2014] Cross, M. E. and Plunkett, E. V. E. (2014). *Resonance and damping*, page 66–69. Cambridge University Press, 2 edition.

[Dingemans, 2000] Dingemans, M. W. (2000). *Water wave propagation over uneven bottoms: Linear wave propagation*, volume 13. World Scientific.

[Drew et al., 2009] Drew, B., Plummer, A. R., and Sahinkaya, M. N. (2009). A review of wave energy converter technology.

[Dufour, 2023] Dufour, D. (2023). Perfect linear absorption of deep water waves through resonance.

[Guo et al., 2022] Guo, B., Wang, T., Jin, S., Duan, S., Yang, K., and Zhao, Y. (2022). A review of point absorber wave energy converters. *Journal of Marine Science and Engineering*, 10(10):1534.

[Holmes, 2009] Holmes, B. (2009). *Tank testing of wave energy conversion systems: marine renewable energy guides*. European Marine Energy Centre.

[Li and Yu, 2012] Li, Y. and Yu, Y.-H. (2012). A synthesis of numerical methods for modeling wave energy converter-point absorbers. *Renewable and Sustainable Energy Reviews*, 16(6):4352–4364.

[Mwasilu and Jung, 2019] Mwasilu, F. and Jung, J.-W. (2019). Potential for power generation from ocean wave renewable energy source: a comprehensive review on state-of-the-art technology and future prospects. *IET Renewable Power Generation*, 13(3):363–375.

[Ogden et al., 2022] Ogden, D., Ruehl, K., Yu, Y.-H., Keester, A., Forbush, D., Leon, J., and Tom, N. (2022). Review of wec-sim development and applications. *International Marine Energy Journal*, 5:293–303.

[Tanaka, 2018] Tanaka, Y. (2018). Active vibration compensator on moving vessel by hydraulic parallel mechanism. *International Journal of Hydromechatronics*, 1:350.

[van Luijk, 2023] van Luijk, R. (2023). Characterizing water wave linearity and absorbing beach performance for a small-scale wave tank.

[Verma and Verma, 2019] Verma, R. and Verma, A. K. (2019). 3d trajectory reconstruction using color-based optical flow and stereo vision. In *Emerging Technologies in Computer Engineering: Microservices in Big Data Analytics: Second International Conference, ICETCE 2019, Jaipur, India, February 1–2, 2019, Revised Selected Papers 2*, pages 70–80. Springer.

[Wei et al., 2017] Wei, Y., Barradas Berglind, J., van Rooij, M., Prins, W., Jayawardhana, B., and Vakis, A. (2017). Investigating the adaptability of the multi-pump multi-piston power take-off system for a novel wave energy converter. *Renewable Energy*, 111:598–610.

[Weller et al., 2015] Weller, S., Davies, P., Vickers, A., and Johanning, L. (2015). Synthetic rope responses in the context of load history: The influence of aging. *Ocean Engineering*, 96:192–204.

[Xu et al., 2019] Xu, S., Wang, S., and Guedes Soares, C. (2019). Review of mooring design for floating wave energy converters. *Renewable and Sustainable Energy Reviews*, 111:595–621.

Appendices

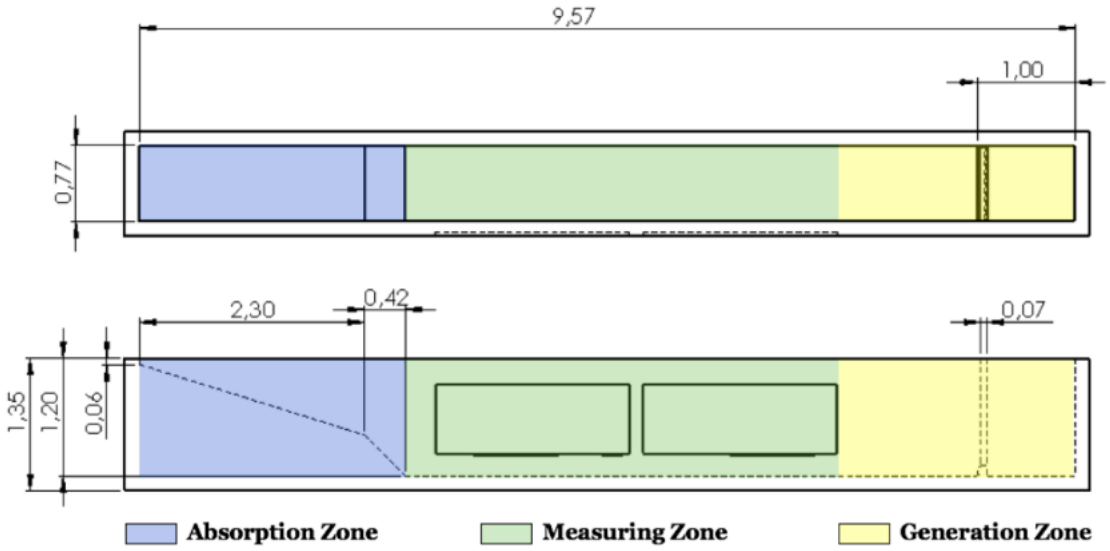

Figure 1: Detailed dimensions of the wave flume used for this research, courtesy of [Dufour, 2023].

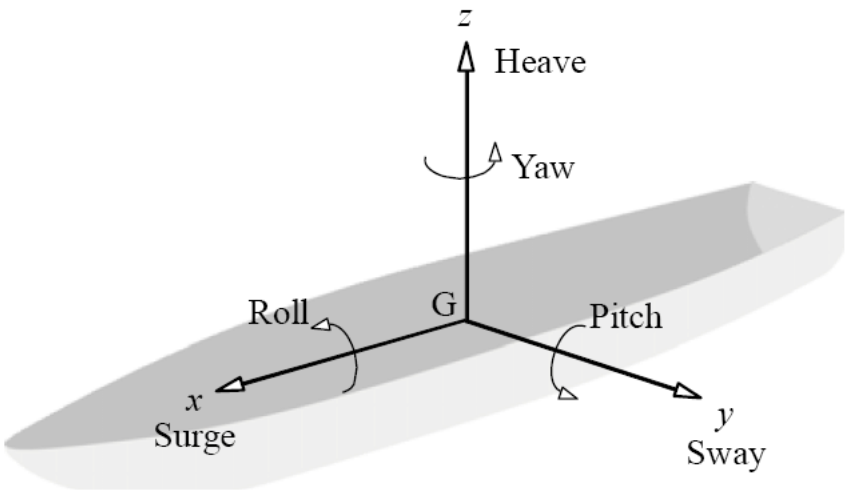

Figure 2: Ship schematic showing labels of motion for 6 degrees of freedom, courtesy of [Tanaka, 2018].

		Valid or Nonvalid Surge values					
Draft	Trial #	20	25	30	35	40	45
D7	1	D7_F20_1	D7_F25_1	D7_F30_1	D7_F35_1	D7_F40_1	D7_F45_1
	2	D7_F20_2	D7_F25_2	D7_F30_2	D7_F35_2	D7_F40_2	D7_F45_2
	3	D7_F20_3	D7_F25_3	D7_F30_3	D7_F35_3	D7_F40_3	D7_F45_3
	4	D7_F20_Avg	D7_F25_Avg	D7_F30_Avg	D7_F35_Avg	D7_F40_Avg	D7_F45_Avg
D8	1	D8_F20_1	D8_F25_1	D8_F30_1	D8_F35_1	D8_F40_1	D8_F45_1
	2	D8_F20_2	D8_F25_2	D8_F30_2	D8_F35_2	D8_F40_2	D8_F45_2
	3	D8_F20_3	D8_F25_3	D8_F30_3	D8_F35_3	D8_F40_3	D8_F45_3
	4	D8_F20_Avg	D8_F25_Avg	D8_F30_Avg	D8_F35_Avg	D8_F40_Avg	D8_F45_Avg
D9	1	D9_F20_1	D9_F25_1	D9_F30_1	D9_F35_1	D9_F40_1	D9_F45_1
	2	D9_F20_2	D9_F25_2	D9_F30_2	D9_F35_2	D9_F40_2	D9_F45_2
	3	D9_F20_3	D9_F25_3	D9_F30_3	D9_F35_3	D9_F40_3	D9_F45_3
	4	D9_F20_Avg	D9_F25_Avg	D9_F30_Avg	D9_F35_Avg	D9_F40_Avg	D9_F45_Avg
D10	1	D10_F20_1	D10_F25_1	D10_F30_1	D10_F35_1	D10_F40_1	D10_F45_1
	2	D10_F20_2	D10_F25_2	D10_F30_2	D10_F35_2	D10_F40_2	D10_F45_2
	3	D10_F20_3	D10_F25_3	D10_F30_3	D10_F35_3	D10_F40_3	D10_F45_3
	4	D10_F20_Avg	D10_F25_Avg	D10_F30_Avg	D10_F35_Avg	D10_F40_Avg	D10_F45_Avg
D11	1	D11_F20_1	D11_F25_1	D11_F30_1	D11_F35_1	D11_F40_1	D11_F45_1
	2	D11_F20_2	D11_F25_2	D11_F30_2	D11_F35_2	D11_F40_2	D11_F45_2
	3	D11_F20_3	D11_F25_3	D11_F30_3	D11_F35_3	D11_F40_3	D11_F45_3
	4	D11_F20_Avg	D11_F25_Avg	D11_F30_Avg	D11_F35_Avg	D11_F40_Avg	D11_F45_Avg
D12	1	D12_F20_1	D12_F25_1	D12_F30_1	D12_F35_1	D12_F40_1	D12_F45_1
	2	D12_F20_2	D12_F25_2	D12_F30_2	D12_F35_2	D12_F40_2	D12_F45_2
	3	D12_F20_3	D12_F25_3	D12_F30_3	D12_F35_3	D12_F40_3	D12_F45_3
	4	D12_F20_Avg	D12_F25_Avg	D12_F30_Avg	D12_F35_Avg	D12_F40_Avg	D12_F45_Avg
D13	1	D13_F20_1	D13_F25_1	D13_F30_1	D13_F35_1	D13_F40_1	D13_F45_1
	2	D13_F20_2	D13_F25_2	D13_F30_2	D13_F35_2	D13_F40_2	D13_F45_2
	3	D13_F20_3	D13_F25_3	D13_F30_3	D13_F35_3	D13_F40_3	D13_F45_3
	4	D13_F20_Avg	D13_F25_Avg	D13_F30_Avg	D13_F35_Avg	D13_F40_Avg	D13_F45_Avg
D14	1	D14_F20_1	D14_F25_1	D14_F30_1	D14_F35_1	D14_F40_1	D14_F45_1
	2	D14_F20_2	D14_F25_2	D14_F30_2	D14_F35_2	D14_F40_2	D14_F45_2
	3	D14_F20_3	D14_F25_3	D14_F30_3	D14_F35_3	D14_F40_3	D14_F45_3
	4	D14_F20_Avg	D14_F25_Avg	D14_F30_Avg	D14_F35_Avg	D14_F40_Avg	D14_F45_Avg
D15	1	D15_F20_1	D15_F25_1	D15_F30_1	D15_F35_1	D15_F40_1	D15_F45_1
	2	D15_F20_2	D15_F25_2	D15_F30_2	D15_F35_2	D15_F40_2	D15_F45_2
	3	D15_F20_3	D15_F25_3	D15_F30_3	D15_F35_3	D15_F40_3	D15_F45_3
	4	D15_F20_Avg	D15_F25_Avg	D15_F30_Avg	D15_F35_Avg	D15_F40_Avg	D15_F45_Avg

Figure 3: Index table of trials, coloured according to whether the Surge data was deemed valid (clear), invalid (red), recalculated (blue), and in-question (yellow), as per Section 5.3.2. All red values were removed from the Surge data set.

Valid or Nonvalid Heave values							
Draft	Trial #	20	25	30	35	40	45
D7	1	D7_F20_1	D7_F25_1	D7_F30_1	D7_F35_1	D7_F40_1	D7_F45_1
	2	D7_F20_2	D7_F25_2	D7_F30_2	D7_F35_2	D7_F40_2	D7_F45_2
	3	D7_F20_3	D7_F25_3	D7_F30_3	D7_F35_3	D7_F40_3	D7_F45_3
	4	D7_F20_Avg	D7_F25_Avg	D7_F30_Avg	D7_F35_Avg	D7_F40_Avg	D7_F45_Avg
D8	1	D8_F20_1	D8_F25_1	D8_F30_1	D8_F35_1	D8_F40_1	D8_F45_1
	2	D8_F20_2	D8_F25_2	D8_F30_2	D8_F35_2	D8_F40_2	D8_F45_2
	3	D8_F20_3	D8_F25_3	D8_F30_3	D8_F35_3	D8_F40_3	D8_F45_3
	4	D8_F20_Avg	D8_F25_Avg	D8_F30_Avg	D8_F35_Avg	D8_F40_Avg	D8_F45_Avg
D9	1	D9_F20_1	D9_F25_1	D9_F30_1	D9_F35_1	D9_F40_1	D9_F45_1
	2	D9_F20_2	D9_F25_2	D9_F30_2	D9_F35_2	D9_F40_2	D9_F45_2
	3	D9_F20_3	D9_F25_3	D9_F30_3	D9_F35_3	D9_F40_3	D9_F45_3
	4	D9_F20_Avg	D9_F25_Avg	D9_F30_Avg	D9_F35_Avg	D9_F40_Avg	D9_F45_Avg
D10	1	D10_F20_1	D10_F25_1	D10_F30_1	D10_F35_1	D10_F40_1	D10_F45_1
	2	D10_F20_2	D10_F25_2	D10_F30_2	D10_F35_2	D10_F40_2	D10_F45_2
	3	D10_F20_3	D10_F25_3	D10_F30_3	D10_F35_3	D10_F40_3	D10_F45_3
	4	D10_F20_Avg	D10_F25_Avg	D10_F30_Avg	D10_F35_Avg	D10_F40_Avg	D10_F45_Avg
D11	1	D11_F20_1	D11_F25_1	D11_F30_1	D11_F35_1	D11_F40_1	D11_F45_1
	2	D11_F20_2	D11_F25_2	D11_F30_2	D11_F35_2	D11_F40_2	D11_F45_2
	3	D11_F20_3	D11_F25_3	D11_F30_3	D11_F35_3	D11_F40_3	D11_F45_3
	4	D11_F20_Avg	D11_F25_Avg	D11_F30_Avg	D11_F35_Avg	D11_F40_Avg	D11_F45_Avg
D12	1	D12_F20_1	D12_F25_1	D12_F30_1	D12_F35_1	D12_F40_1	D12_F45_1
	2	D12_F20_2	D12_F25_2	D12_F30_2	D12_F35_2	D12_F40_2	D12_F45_2
	3	D12_F20_3	D12_F25_3	D12_F30_3	D12_F35_3	D12_F40_3	D12_F45_3
	4	D12_F20_Avg	D12_F25_Avg	D12_F30_Avg	D12_F35_Avg	D12_F40_Avg	D12_F45_Avg
D13	1	D13_F20_1	D13_F25_1	D13_F30_1	D13_F35_1	D13_F40_1	D13_F45_1
	2	D13_F20_2	D13_F25_2	D13_F30_2	D13_F35_2	D13_F40_2	D13_F45_2
	3	D13_F20_3	D13_F25_3	D13_F30_3	D13_F35_3	D13_F40_3	D13_F45_3
	4	D13_F20_Avg	D13_F25_Avg	D13_F30_Avg	D13_F35_Avg	D13_F40_Avg	D13_F45_Avg
D14	1	D14_F20_1	D14_F25_1	D14_F30_1	D14_F35_1	D14_F40_1	D14_F45_1
	2	D14_F20_2	D14_F25_2	D14_F30_2	D14_F35_2	D14_F40_2	D14_F45_2
	3	D14_F20_3	D14_F25_3	D14_F30_3	D14_F35_3	D14_F40_3	D14_F45_3
	4	D14_F20_Avg	D14_F25_Avg	D14_F30_Avg	D14_F35_Avg	D14_F40_Avg	D14_F45_Avg
D15	1	D15_F20_1	D15_F25_1	D15_F30_1	D15_F35_1	D15_F40_1	D15_F45_1
	2	D15_F20_2	D15_F25_2	D15_F30_2	D15_F35_2	D15_F40_2	D15_F45_2
	3	D15_F20_3	D15_F25_3	D15_F30_3	D15_F35_3	D15_F40_3	D15_F45_3
	4	D15_F20_Avg	D15_F25_Avg	D15_F30_Avg	D15_F35_Avg	D15_F40_Avg	D15_F45_Avg

Figure 4: Index table of trials, coloured according to whether the Heave data was deemed valid (clear), invalid (red), recalculated (blue), as per Section 5.3.2. All red values were removed from the Heave data set.

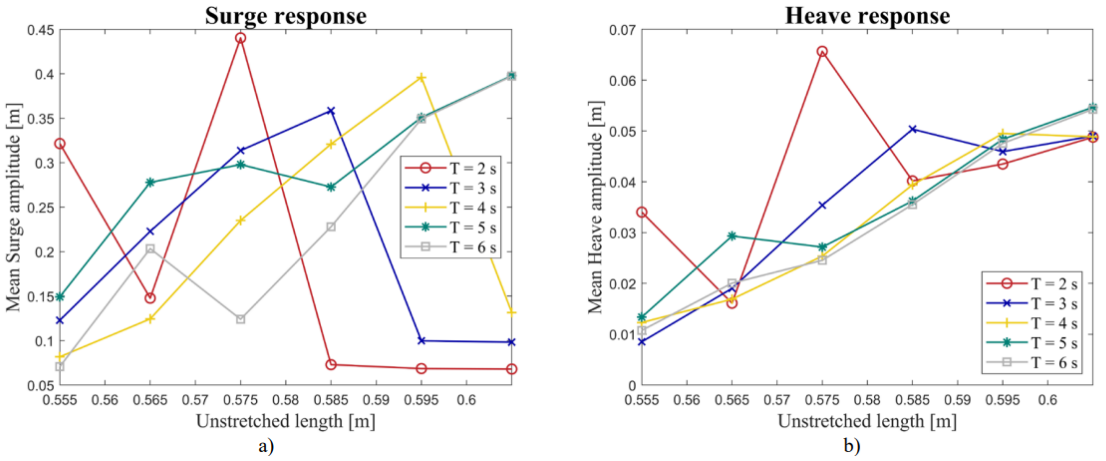

Figure 5: Surge and Heave amplitude responses recorded in [Asiikkis et al., 2023].

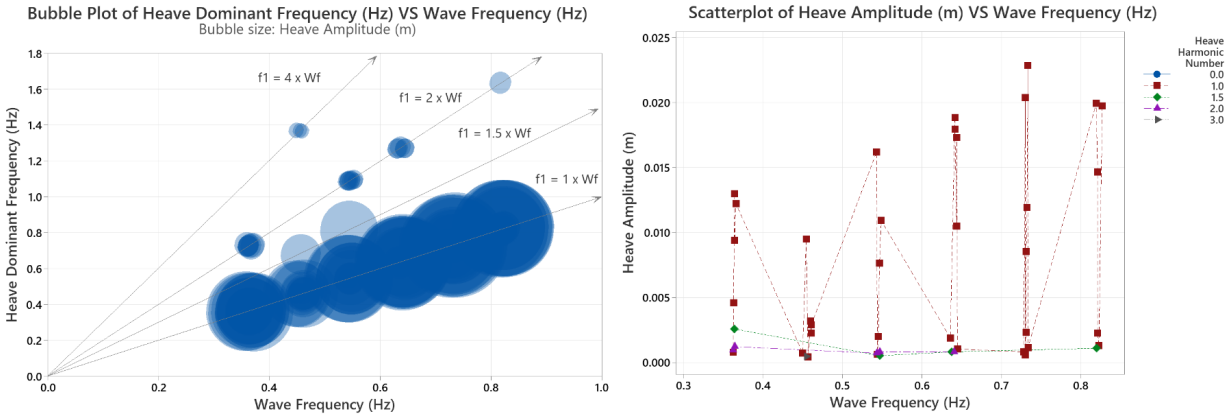

Figure 6: Figures for Heave, equivalent to Figures 6.6 and 6.7 for Surge, showing far different behaviour. These were outside the scope of the project for analysis, but may be of interest to look at.

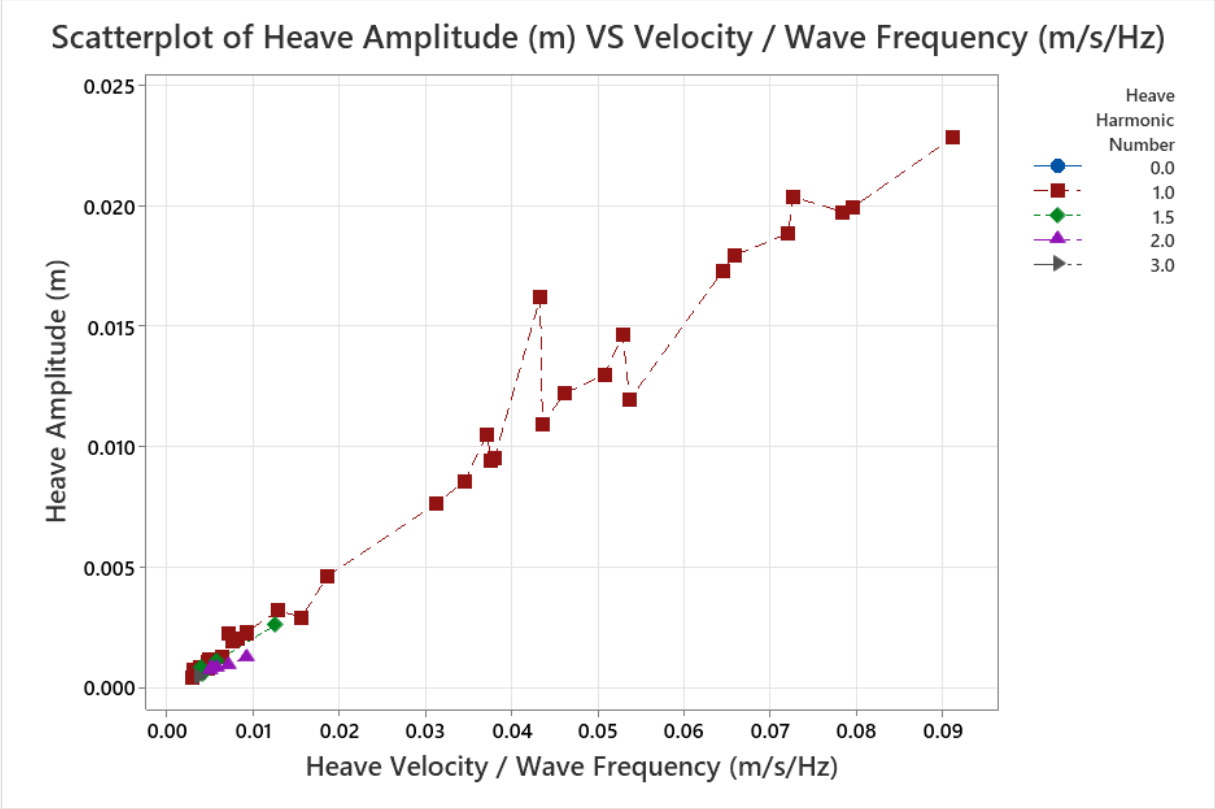

Figure 7: Figure for Heave, equivalent to Figure 6.8 for Surge. This was outside of the scope for analysis, but may be of interest to look at.